Electroacoustic Efficiency of the Thermoacoustic Transducer based on r-GO Folio

Master Thesis

Miaoqing Sheng

Fachgebiet Audiokommunikation
Institut für Sprache und Kommunikation
Fakultät I - Geistwissenschaft
TU Berlin

March 2018

1.Supervisor Prof. Dr. Stefan Weinzierl
Fachgebiet Audiokommunikation
TU Berlin
2.Supervisor Prof. Dr. Aleksander Gurlo
Fachgebiet Keramische Werkstoffe
TU Berlin
3.Supervisor Dipl.-Ing. Florian Straube
Fachgebiet Audiokommunikation
TU Berlin

Contents

Eidesstattliche Erklärung

Hiermit versichere ich gegenüber der Fakultät I der Technischen Universität Berlin, dass ich die vorliegende Arbeit selbstständig verfasst und keine anderen als die angegebenen Quellen und Hilfsmittel benutzt habe. Alle Ausführungen, die anderen veröffentlichen oder nicht veröffentlichen Schriften wörtlich oder sinngemäß entnommen wurden, habe ich kenntlich gemacht. Die Arbeit hat in gleicher oder ähnlicher Fassung noch keiner anderen Prüfungsbehörde vorgelegen.

Berlin, den 27. März 2018 _____

Miaoqing Sheng

Abstract

The thermoacoustic phenomenon has been around since late 19th century (Preece, 1879) but drew little attention at the time. In 2008, the exploration of some newly discovered nanomaterial has brought back a new interest in thermoacoustic (Xiao et al., 2008). Despite many approaches using different assemblies of Carbon Nano Tube (CNT) or graphene while discussing their possibility of becoming the next candidate of a thermoacoustic transducer, the main obstacle for a practical application remains, namely the low electroacoustic efficiency. The primary purpose of this master thesis is to experimentally explore the electroacoustic efficiency of a specific graphene assembly using a controllable signal and looking for possible factors that may affect its efficiency. For this purpose, the impedance of different samples has been tested, the sound power of each sample was then measured in an anechoic chamber. A prototype circuit drives the samples and provides an adjustable DC-offset to reconstruct the correct frequency. The measured electroacoustic efficiency was compared with similar research and possible reasons for discrepancy and improvements are given for a better efficiency performance of the future thermoacoustic transducer.

Zusammenfassung

Das thermoakustische Phänomen wurde bereits im späten 19. Jahrhundert entdeckt (Preece, 1879), wurde aber zu dieser Zeit wenig beachtet. Bis 2008 brachte die Erforschung einiger neu entdeckter Nanomaterialien erstmals die thermoakustische Rückgewinnung (Xiao et al., 2008). Trotz vieler Ansätze, die verschiedene Anordnungen von Carbon Nano Tube (CNT) oder Graphen verwenden, und dabei die Möglichkeit diskutieren, der nächste Kandidat eines thermoakustischen Wandlers zu werden, bleibt das Haupthindernis für eine praktische Anwendung, nämlich der geringe elektroakustische Wirkungsgrad. Der Hauptzweck dieser Masterarbeit ist die experimentelle Untersuchung des elektroakustischen Wirkungsgrads einer bestimmten Graphenanordnung unter Verwendung eines steuerbaren Signals und die Suche nach möglichen Faktoren, die den Wirkungsgrad beeinflussen können. Zu diesem Zweck wurde die Impedanz verschiedener Proben getestet, und die Schallleistung jeder Probe wird dann in einem reflexionsarmen Raum (RAR) gemessen, wobei eine Prototypschaltung verwendet wird, die einen einstellbaren Gleichstrom-Offset anwendet, um die richtige Frequenz wiederherzustellen. Der gemessene elektroakustische Wirkungsgrad wird mit ähnlichen Forschungen verglichen. Schließlich werden einige mögliche Gründe für Diskrepanzen und Verbesserungen für einen besseren Wirkungsgrad zukünftiger thermoakustischer Wandler vorgeschlagen.

1. Introduction

The thermoacoustic phenomenon was first noticed in the late 19th century when William Henry Preece (Preece, 1879) observed the sound emitting due to heating and cooling of a metal wire. Decades later, Arnold and Crandall conducted several qualitative experiments based on their mathematical model (Arnold and Crandall., 1917). The theory and experiments confirmed the observation of Preece, and they suggested therefore that the general characters of those materials, could be utilized as a thermoacoustic sound emitter:

"To secure appreciable amplitudes with currents of ordinary magnitude it is essential that the conductor be very thin; its heat capacity must be small, and it must be able to conduct at once to its surface the heat produced in its interior, in order to follow the temperature changes produced by a rapidly varying current." (Arnold and Crandall., 1917)

Since such peculiar conditions were so difficult to be fulfilled with traditional materials at that time, this discovery was soon forgotten, and there was no further research concerning this topic until 2008. Accompanied by the newly discovered Nano-material: carbon nanotube (CNT) and several experiments conducted by Xiao Lin (Xiao et al., 2008) the thermoacoustic effect was rediscovered.

Unlike other sound emitting devices, such as dynamic loudspeakers or earphones, electrostatic earphones etc., which convert electrical energy into mechanical energy to produce acoustic vibration in the surrounding medium (Gas in most cases), the thermoacoustic device converts electrical energy to Joule heat, which then causes the synchronous oscillation of temperature in surrounding mediums ultimately producing the sound wave.

In other words, the conventional acoustic transducers only perform adiabatic volume-work, while the thermo-acoustic transducers only generate heat. However, in both cases the periodic variation of internal energy results in pressure amplitudes (Daschewski et al., 2013).

Despite several advantages, such as extremely low weight and thickness, no post-oscillation (Daschewski et al., 2013), pure resistive under MHz (Xiao et al., 2008), there are two primary drawbacks comparing with conventional transducer:

a. the low energy conversion efficiency.

Almost all thermoacoustic transducers reported so far have not yet achieved the same efficiency level of conventional transducers. Moreover, since there is also no uniform standard, most of the works did not mention or calculate the efficiency. Besides the theoretical research of fundamental efficiency derived from Green's function (Vesterinen et al., 2010), and a theoretical formula (Xiao et al., 2011), a review of thermoacoustic efficiency from different

assemblies and material was given by (Aliev et al., 2015). A rough calculation of efficiency could later be found in (Zhang et al., 2017), giving the efficiency of graphene woven fabrics along with some other thermoacoustic transducers from 0.0006% up to 0.1%. On the other hand, the efficiency of conventional transducers, i.e., dynamic loudspeaker, is around 1%, and positive proportional to its power level. The low efficiency of the thermoacoustic transducer may be the primary obstacle for a practical application.

b. Correct reconstruction of Signals

As suggested by theoretical derivation, the sound pressure created by a thermoacoustic transducer is proportional to electric power rather than voltage, and since the electric power is direction insensitive, it results in an inherent "2nd-harmonic distortion". This affects mostly the quality of acoustic signal but can also influence the efficiency of transducer depending on the methods of signal reconstruction.

In this master thesis, the electroacoustic efficiency of the thermoacoustic transducer which was made from an r-GO assembly is experimentally examined. The primary purpose is to prove the basic principles of thermoacoustic and to empirically explore the potential of r-GO assembly as a thermoacoustic transducer.

2. Thermoacoustic

2.1. Concept and Terms

Although the term "Thermoacoustic" has already been used through decades and there were plenty of researches concerning this concept or its applications, such as thermoacoustic engine, the precise definition of this term is still elusive.

In history, there were two approaches involving thermoacoustic. One of them was inspired by the phenomenon of heat generated sound during glass blowing. A device called Riijke tube demonstrated this phenomenon by heating a wire mesh in a metal tube and created loud sound. The other approach, which inspires this work, is to apply the thermoacoustic in a more controllable way which could transmit audio signals like other electroacoustic transducers.

Therefore, a description for thermoacoustic which suits the context of this work could be:

"Thermoacoustic is the interaction between electric, thermal and mechanic energy, which converts an electric signal into acoustic wave utilizing controllable temperature oscillation."

As for the thermoacoustic transducer, essentially it is an electroacoustic transducer, but its energy conversion takes another path which distinguishes it from the electrodynamic or electrostatic transducer. Those principles are schematically depicted in Figure 2.1
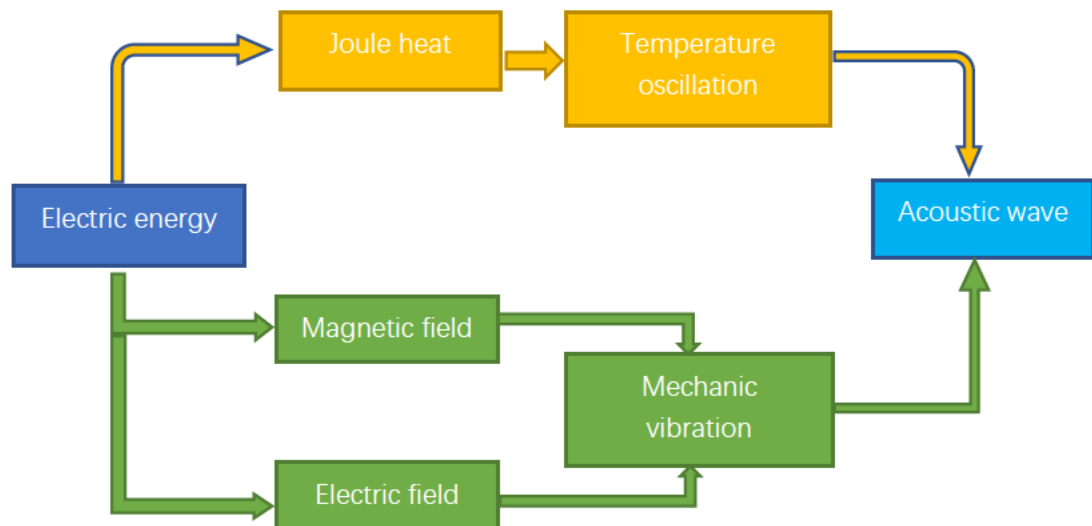

Figure 2.1 Principle of Transducers

Based on this principle, all the thermoacoustic transducer, no matter what material it is, has

one trait in common: the transducer itself has no vibrating structure. The vibration happens directly in surrounding gaseous medium triggered by temperature oscillation.

A thermoacoustic transducer could, therefore, be described: a transducer without any moveable structure, which converts electric energy into mechanical energy in the form of the acoustic wave by rapidly conducting Joule heat into surrounding gaseous medium.

To rapidly conducting the Joule heat into the gaseous medium which triggers temperature oscillation according to the input electric signal, the material of the transducer and its micro-structure are crucial. Until now, suitable material includes platinum and aluminum folio or nanowire, but mostly are newly discovered Nano-material such as Carbon Nano Tube (CNT) and Graphene. The electroacoustic efficiency of the transducer depends strongly on the thermal characters of the materials as well as its microstructure. A general description of the r-GO folio for this article is given in chapter 3.1.

Another inherent trait, as well as one of the primary drawbacks of thermoacoustic, is the so-called "double frequency effect". According to the basic theory of thermoacoustic, the frequency of the acoustic wave is always double of the frequency of the electric signal, given no other precautions. A simple explanation of this phenomenon is, the sound pressure produced by temperature oscillation is proportional to input electric power, rather than electric voltage. A more sophisticated derivation together with some precaution which could minimize the distortion brought by this phenomenon will be given in chapter 2.2

2.2. Frequency Reconstruction

If the frequency of output signal cannot be correctly reconstructed, the efficiency of the transducer is meaningless. On the other hand, the efficiency of the transducer also depends on different reconstruction precautions. It is thus necessary to examine the reason for the frequency distortion and some of the precautions.

2.2.1.   A Simplified Theory and the Doubled Frequency

As suggested by (Xiao et al., 2008), the relation of sound pressure p and the input electric power P can be described using following equation:

$$p_{rms} = \frac{\sqrt{\alpha}\rho_0}{2\sqrt{\pi}T_0} \cdot \frac{1}{r} \cdot P_{input} \cdot \frac{\sqrt{f}}{c_s} \cdot \frac{\frac{f}{f_2}}{\sqrt{\left(1+\sqrt{\frac{f}{f_1}}\right)^2 + \left(\frac{f}{f_2}+\sqrt{\frac{f}{f_1}}\right)^2}} \tag{1}$$

This complicated equation can be breakdown into following terms:

a. $\frac{\sqrt{\alpha}\rho_0}{2\sqrt{\pi}T_0}$, it describes the relation of p_{rms} and the density, temperature and thermal diffusivity of the ambient gas, constant

b. $\frac{1}{r}$, p_{rms} decreases as the distance between the transducer and the reference point, i.e. 6 dB SPL per distance doubling.

c. $\frac{\sqrt{f}}{c_s}$, p_{rms} is proportional to square root of input frequency and invers-proportional to the heat capacity per unit area (HCPUA)

d. $\frac{\frac{f}{f_2}}{\sqrt{(1+\sqrt{\frac{f}{f_1}})^2 + (\frac{f}{f_2}+\sqrt{\frac{f}{f_1}})^2}}$, the correction factor for material, constant for given material and frequency (a more detail explain for coefficients f_1 and f_2 is given in chapter 2.2.2).

The thermodynamic constants using in a. to d. can be found in Appendix 1.

In other words, considering the identical condition of surrounding air, for the folio with same thermal constants, **the p_{rms} is proportional to P_{input}, given constant f;**

For the instantaneous value of sound pressure, it is easy to prove:

$$p_A(t) = a \cdot P_E(t) \tag{2}$$

Where a represents all the time irrelevant coefficients and constants described in a. to d. above. $p_A(t)$ and $P_E(t)$ is the instantaneous sound pressure and electric power, respectively.

and therefore, **the sound pressure $p_A(t)$ should have the wave form of $P_E(t)$**

For $P_E(t)$, the expression is trivial:

$$P_E(t) = U(t)I(t) \tag{3}$$

More specific, for a single sinusoid tone:

$$P_E(t) = \hat{U}\sin(\omega t)\,\hat{I}\sin(\omega t) = \hat{U} \cdot \hat{I} \cdot (\tfrac{1}{2} - \tfrac{1}{2}\cos(2\omega t))^1 \tag{4}$$

This equation shows, the input electric power is comprised of a DC term, which contributes nothing to signal, and a cosines term with doubled frequency.
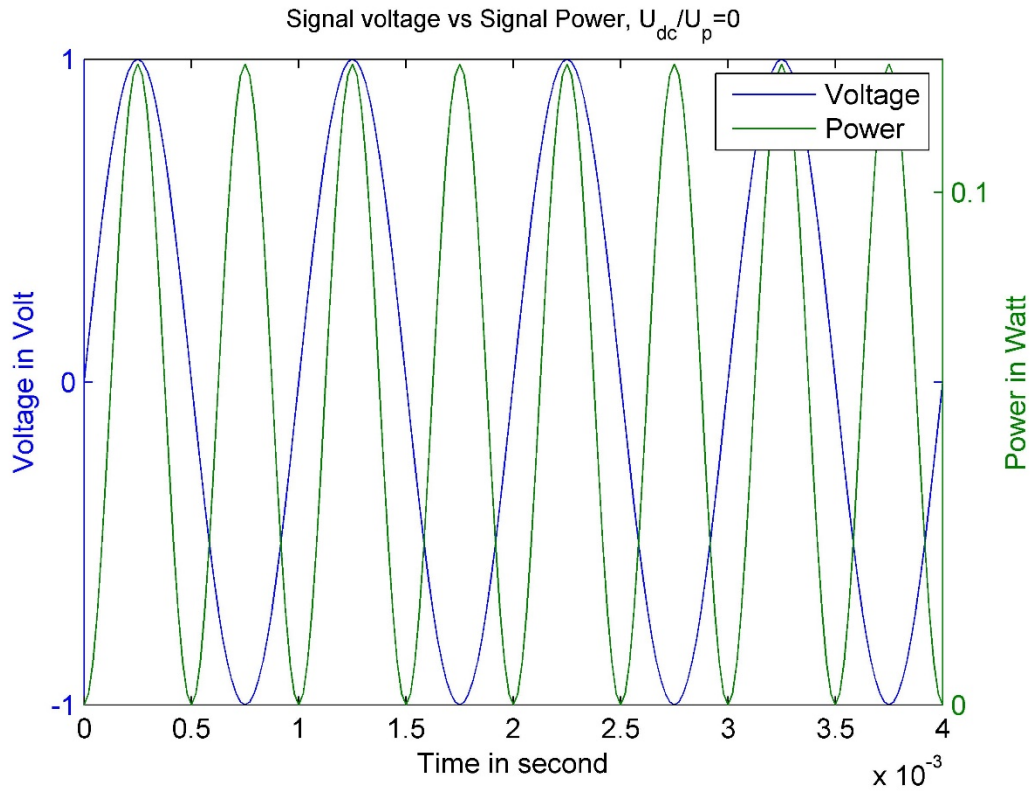

Figure 2.2 Voltage vs Power, no DC-Offset

In this case, the total harmonic distortion of the acoustic signal reconstructed by thermoacoustic transducer should be considered infinitive since no original frequency is reconstructed.

2.2.2. Correction with DC-Offset
This is a mathematically straightforward method to minimize the doubled frequency, as suggested by (Arnold and Crandall., 1917).

The Eq. (3) could be reformulated into:

---

[1] The derivation assumes the current and voltage is in phase, which means the transducer can be treated as pure resistive, this will be proved in chapter 3.3

$$P_{\mathrm{E}}(t) = \widehat{U}\sin(\omega t)\,\widehat{I}\sin(\omega t) = \frac{(\widehat{U}\cdot\sin(\omega t))^2}{R} \tag{5}$$

Where R is the DC-Resistance of the transducer

With superposed DC-offset Voltage U_0:

$$P_{\mathrm{E}}(t) = \frac{(\widehat{U}\cdot\sin(\omega t)+U_0)^2}{R} = \frac{(\frac{1}{2}\widehat{U}^2 - \frac{1}{2}\widehat{U}^2\cos(2\omega t)+2\widehat{U}\cdot U_0\sin(\omega t)+U_0{}^2)}{R} \tag{6}$$

Now the equation is comprised of three terms:

a. Constant voltage: $\dfrac{\frac{1}{2}\widehat{U}^2 + U_0{}^2}{R}$, which has no contribution to signal, only constantly heat the transducer;

b. Doubled frequency: $\dfrac{-\frac{1}{2}\widehat{U}^2\cos(2\omega t)}{R}$, whose amplitude is irrelevant to the DC-offset voltage; and

c. Original frequency: $\dfrac{2\widehat{U}\cdot U_0\sin(\omega t)}{R}$, whose amplitude is determined by the amplitude of the input signal and the DC-offset voltage.

The ratio of the original frequency and doubled frequency is thus:

$$\left|\frac{2\widehat{U}\cdot U_0}{-\frac{1}{2}\widehat{U}^2}\right| = \frac{4U_0}{\widehat{U}} \tag{7}$$

Or

$$20\log\left(\frac{4U_0}{\widehat{U}}\right) = 20\log\left(\frac{U_0}{U_{\mathrm{rms}}}\right) + 9.03\ \mathrm{dB} \tag{8}$$

As shown in Fig.2-Fig.8, as the ratio of DC Voltage to signal amplitude increases, the similarity of the power oscillation to the voltage oscillation of the signal in time domain increases.
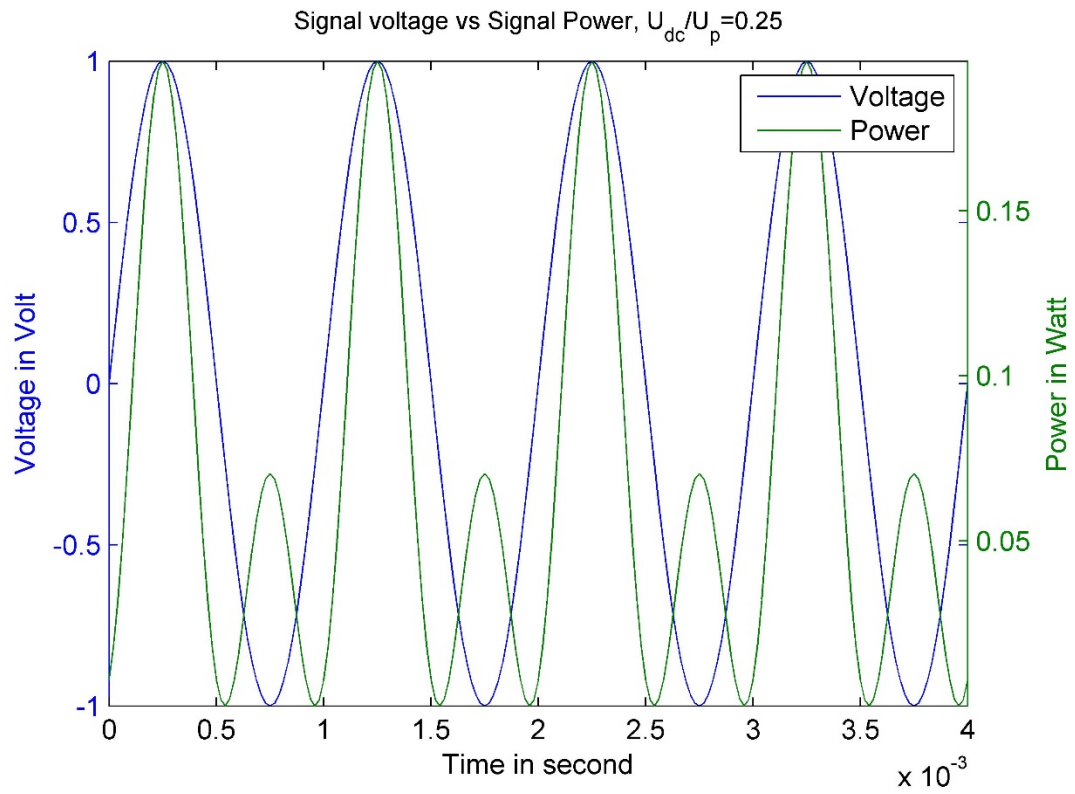
Figure 2.3 Voltage vs. Power, $\dfrac{U_{\text{dc}}}{U_{\text{ac,peak}}} = 0.25$
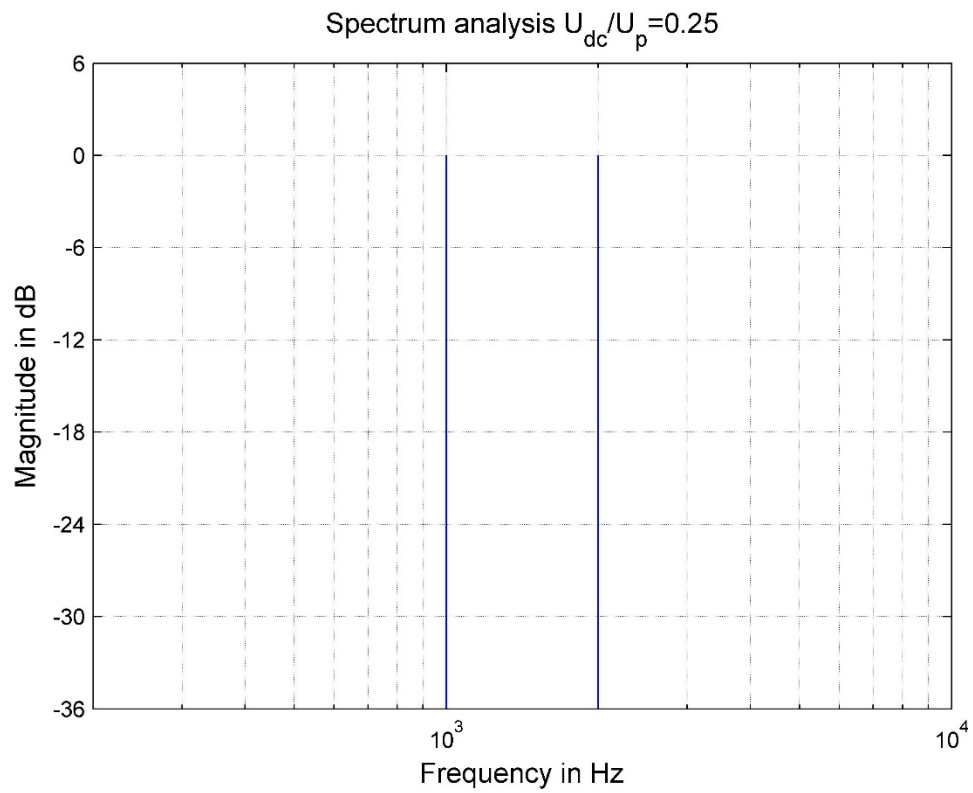
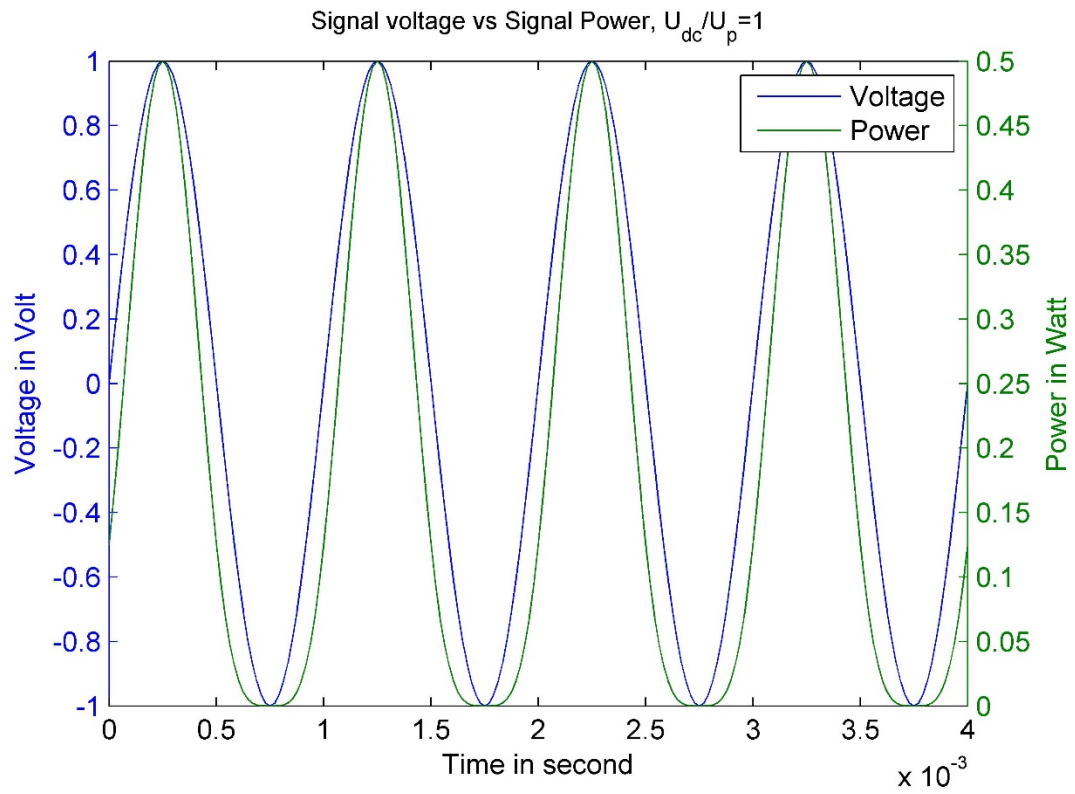Figure 2.4 Spectrum Analysis, $\dfrac{U_{\text{dc}}}{U_{\text{ac,peak}}} = 0.25$

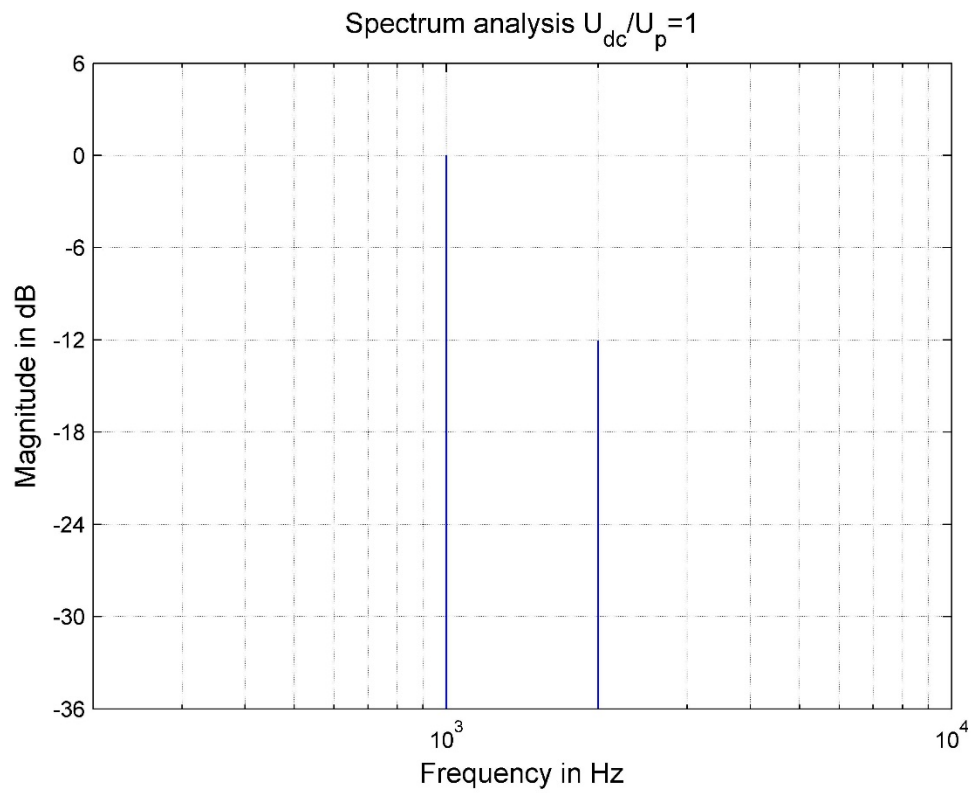Figure 2.5 Voltage vs. Power, $\dfrac{U_{dc}}{U_{ac,peak}} = 1$

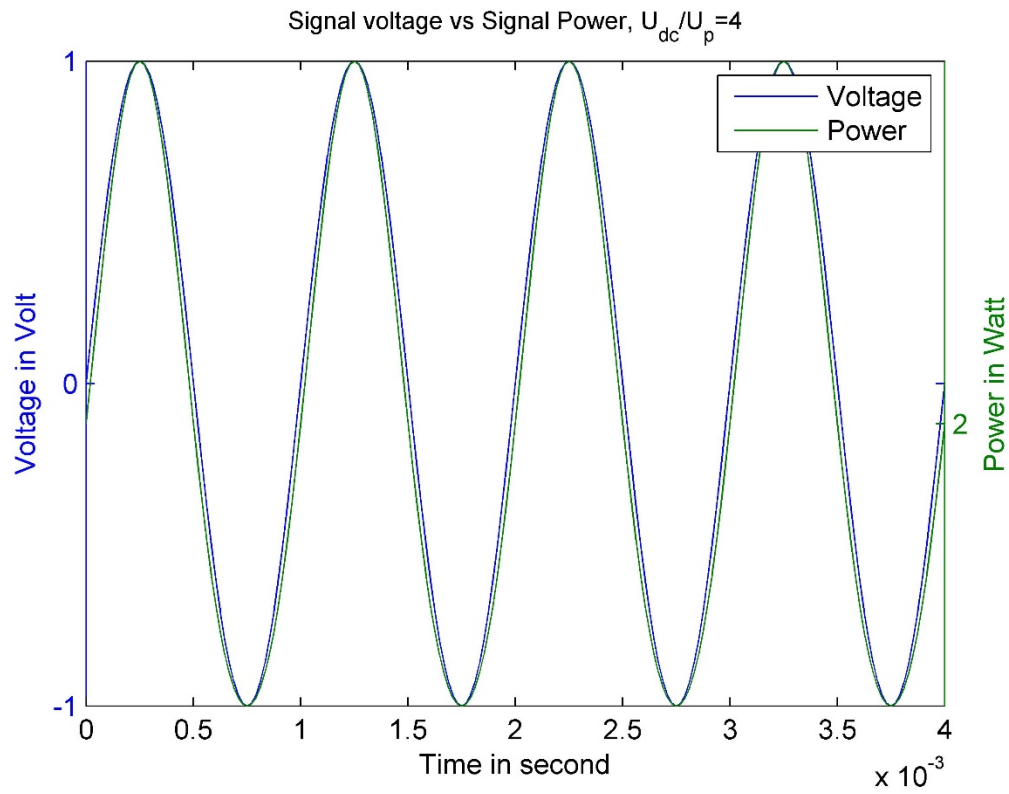Figure 2.6 Spectrum Analysis, $\dfrac{U_{dc}}{U_{ac,peak}} = 1$
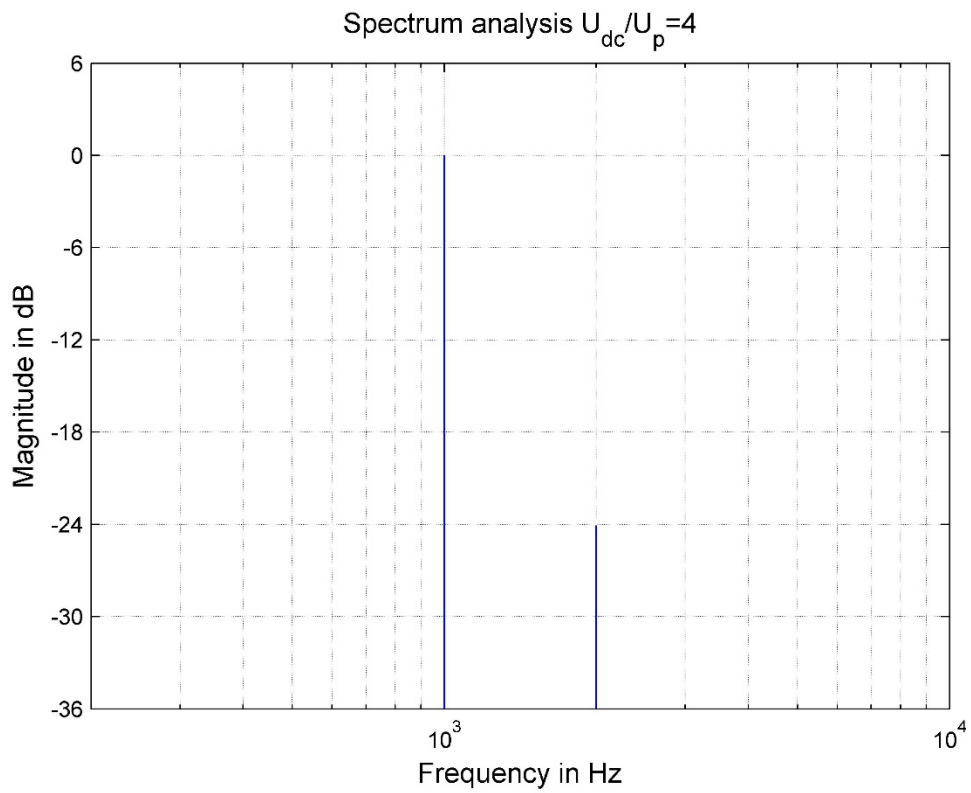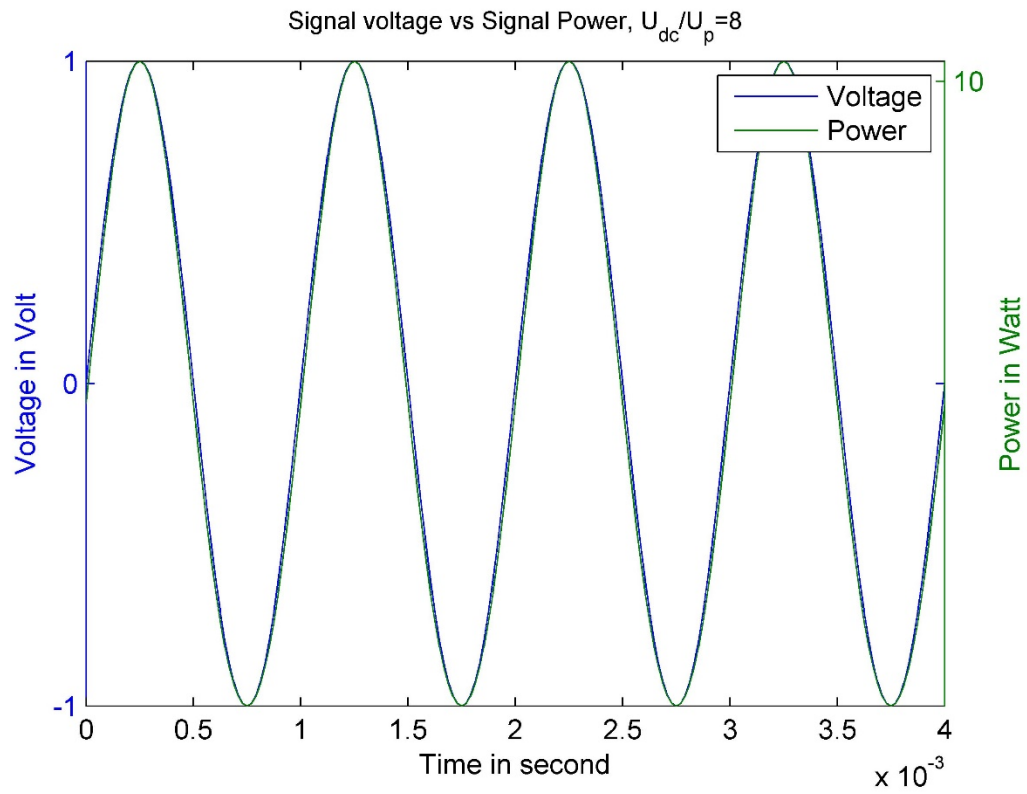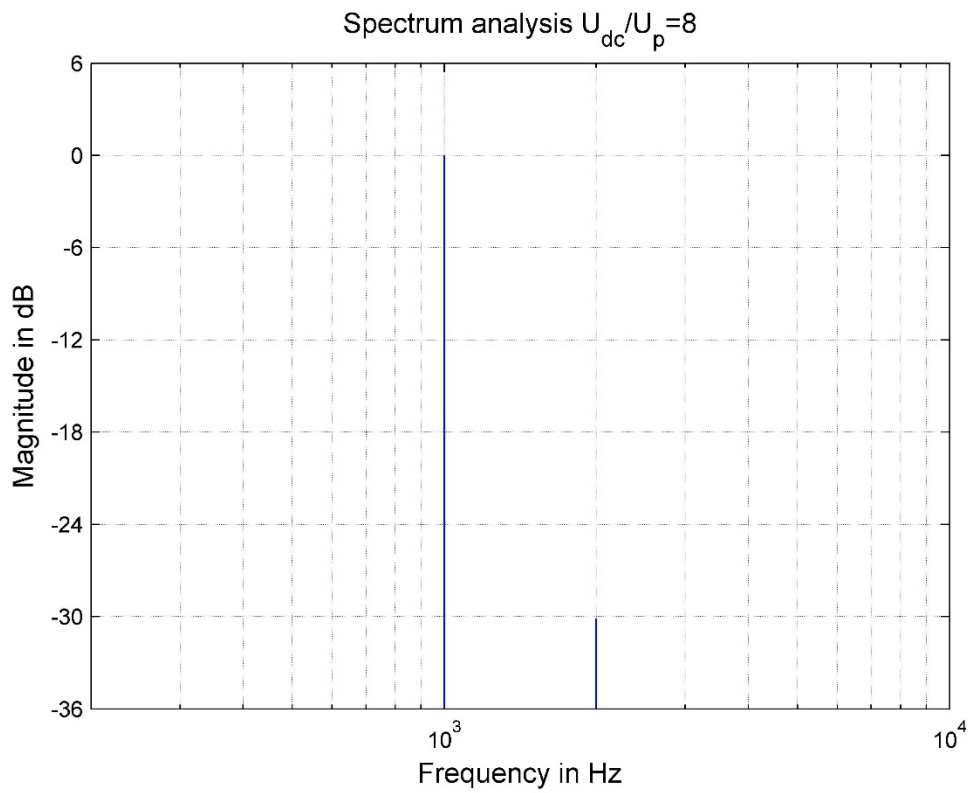
Figure 2.7 Voltage vs. Power, $\dfrac{U_{\text{dc}}}{U_{\text{ac,peak}}} = 4$

Figure 2.8 Spectrum Analysis, $\dfrac{U_{\text{dc}}}{U_{\text{ac,peak}}} = 4$

Figure 2.9 Voltage vs. Power, $\dfrac{U_{\mathrm{dc}}}{U_{\mathrm{ac,peak}}} = 8$

Figure 2.10 Spectrum Analysis, $\dfrac{U_{\mathrm{dc}}}{U_{\mathrm{ac,peak}}} = 8$

A further analysis using Eq. (8) shows the trend of the THD with different combinations of U_{dc} and $U_{ac,peak}$ in Figure 2.11
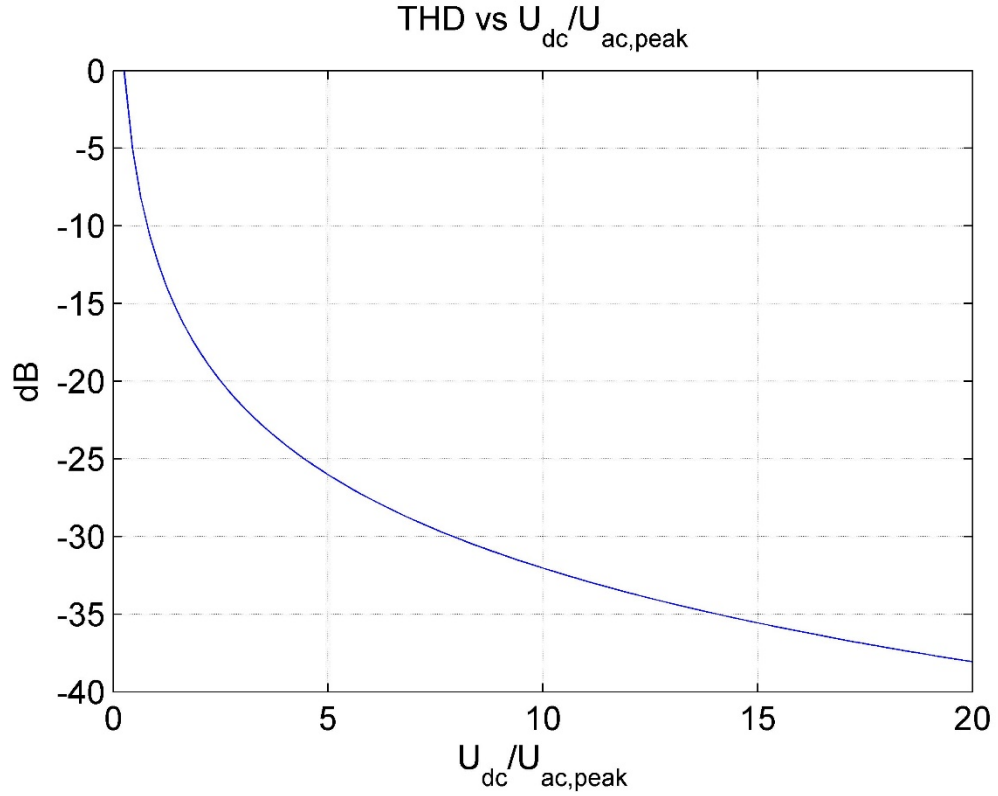
Figure 2.11 THD to DC-offset

It seems that if the ratio of DC-Voltage to signal amplitude increases endlessly, the doubled frequency will eventually become neglectable, albeit there are two reasons which make the infinitive increasing of DC-offset unpractical:

a. The DC-offset voltage U_0 in constant voltage term of Eq. (6) is square rather than linear as it in original frequency term, and the amplitude of constant Voltage thus increases more rapid than the amplitude of original frequency. This will strongly deteriorate the performance of efficiency; and

b. The heat brought by the constant voltage could destroy the transducer, if U_0 is set too high.

Because of such trade-off, the DC-offset voltage must be carefully adjusted. Still, it is among the most straightforward methods of minimizing the doubled frequency and therefore be utilized in the primary test.

2.3. Theoretical Calculation of SPL

Since the thermoacoustic is a newly emerging research area, a uniformly applicable theoretical model has not yet been proposed. On the other hand, many new materials with different micro-structure have already been tested, and certain amendments or corrections have been introduced into the original theory to explain the discrepancy between theoretical calculation and practical observation. Nonetheless, through some of the theories, a better understanding of the whole picture of the thermoacoustic could be achieved.

2.3.1.   The Sound Pressure Calculation from (Arnold and Crandall., 1917)

The pioneer of the thermoacoustic gave the following equations to calculate the sound pressure change at any point in the field

$$\Pi = \frac{-\rho_0 \alpha \xi_{max} \cdot 2\pi f}{2\pi r} \sin(pt - \frac{2\pi r}{\lambda}) \tag{9}$$

$$\xi^2_{max} = p\xi_{max} = \frac{4.0 \times 10^{-9} R^2 I_0^2 i^4}{\alpha^2 \gamma^2 f^3} \tag{10}$$

Substitute Eq. (10)into Eq. (9) and re-organize:

$$\Pi = -\frac{\rho_0 \times 2 \times 10^{-4.5} R I_0 i}{r \gamma f^{1/2}} \sin\left(pt - \frac{2\pi r}{\lambda}\right) \tag{11}$$

Where

ρ_0: density of air,

R: resistance of Pt thin film,

I_0: DC-current,

I: AC-current peak value,

R: distance between observation point of the center of Pt thin film,

γ: heat capacity per unit area of Pt,

f: input AC-current frequency,

p: angular frequency $p=2\pi f$ and

λ: temperature wave-length, $\lambda = \sqrt{\frac{8\pi^2 k}{p}}$, k is the thermal diffusivity

2.3.2.   The Equation from (Xiao et al., 2008)

Based on the same physical picture of Arnold and Crandall but giving up some of the unreasonable assumptions, a more explicit expression of the root-mean-square sound pressure produced by the thermoacoustic transducer is given as Eq. (12)

$$p_{rms} = \frac{\sqrt{\alpha}\rho_0}{2\sqrt{\pi}T_0} \cdot \frac{1}{r} \cdot P_{input} \cdot \frac{\sqrt{f}}{c_s} \tag{12}$$

Where

α: Thermal diffusivity of air, $\alpha = \kappa/\rho_0 c_p$

ρ_0: Density of air

κ: Thermal conductivity of air

c_p: Specific heat capacity or heat capacity per unit mass of air

T_0: Temperature of the air in far-field

r : Distance between thermoacoustic transducer and measure point

P_{input}: Input electric power

f: Frequency of input signal

c_s: Heat capacity per unit area of the thermoacoustic transducer

Noticing the discrepancy between the experiment result and the theoretical prediction from equation (10), a new factor is introduced into the energy conversion model of Arnold and Crandall, thus higher consistency of experiment and theory is achieved:

$$p_{rms} = \frac{\sqrt{\alpha}\rho_0}{2\sqrt{\pi}T_0} \cdot \frac{1}{r} \cdot P_{input} \cdot \frac{\sqrt{f}}{C_s} \cdot \frac{\frac{f}{f_2}}{\sqrt{\left(1 + \sqrt{\frac{f}{f_1}}\right)^2 + \left(\frac{f}{f_2} + \sqrt{\frac{f}{f_1}}\right)^2}}$$

where

$$f_1 = \frac{\alpha\beta_0^2}{\pi\kappa^2}, \ f_2 = \frac{\beta_0}{\pi c_s}$$

β_0: Rate of the heat loss per unit area of the thermoacoustic transducer (due to conduction, convection and radiation) per unit rise in temperature of the transducer above of that of its surroundings.

This is the Eq. (1), which has already been mentioned in chapter 2.1.1.

Hence there is a critical condition for omitting the additional coefficient:

$$\frac{\frac{f}{f_2}}{\sqrt{\left(1 + \sqrt{\frac{f}{f_1}}\right)^2 + \left(\frac{f}{f_2} + \sqrt{\frac{f}{f_1}}\right)^2}} = 1,$$

Which equals to

$$\frac{f}{f_2} \gg \sqrt{\frac{f}{f_1}}, \text{ and thus}$$

$$f \gg \kappa^2/\pi\alpha c_s^2 \tag{13}$$

In other words, the heat capacity per unit area decides the critical frequency, above which the additional coefficient must be taken into consideration. For 1-layer CNT whose $c_s = 5 \times 10^{-3}$ J/m$^2 \cdot$ K, the critical frequency $f \gg 1.65$ MHz, which means the additional

coefficient must be apply for the whole audible frequency range.

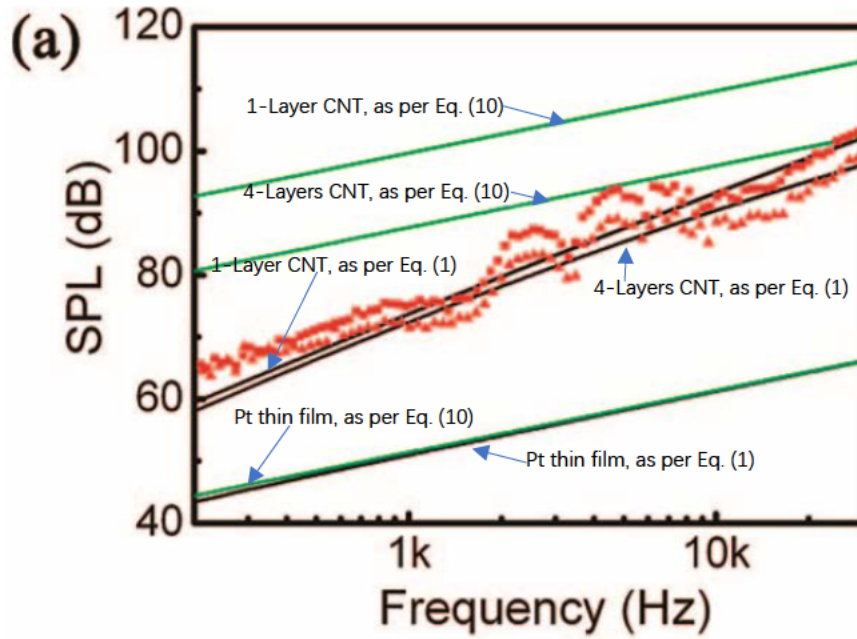According to Eq. (1) and Eq. (12), a comparison has also been given as in Figure 2.12

Figure 2.12 Comparing SPL from Eq. (1) and Equation (12) (Xiao et al., 2008)

The input power is given constant at 4.5 W, SPL measured at distance of 5 cm.

In other words, considering the identical condition of surrounding air, for the folio with same thermal constants, **the p_{rms} is proportional to $\sqrt{f}$, given constant P_{input}.**

A theoretical calculation compared to the measured SPL could be found in Chapter 5.3.

3. r-GO Folio

3.1. Preparation and Characterization of r-GO Folio

Graphene is one of the star nanomaterials in recent years. The few and signal layer graphene was first obtained using mechanical exfoliation, or "Scotch-tape" method (Novoselov, 2004). Nowadays there are different methods which can make different assemblies using graphene. One of the most important ways is epitaxial chemical vapor deposition (CVD). Although this method can provide high quality single or few-layer graphene, it is less efficient.

The reduced-Graphene Oxide (r-GO) folio using in this article utilizes another approach, which uses graphene oxide (GO) chemically prepared from graphite flakes (Marcano et al., 2010). The GO flakes could then be assembled into paper-like or folio-like structure by filtrating the graphene oxide colloidal dispersion in water through an Anodisc membrane filter(Dikin et al., 2007). At last the oxide groups of the GO are removed in high-temperature Nitrogen or Argon environment. A schematic preparation route can be summarized as follows:
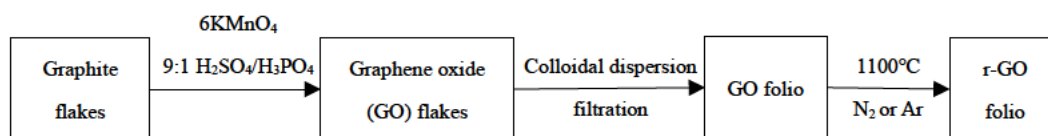
Figure 3.1 Preparation Route of r-GO Folio

Typically, the prepared GO folio has a sandwich structure shown in Figure 3.2

Figure 3.2 Schematic Drawing of GO Folio
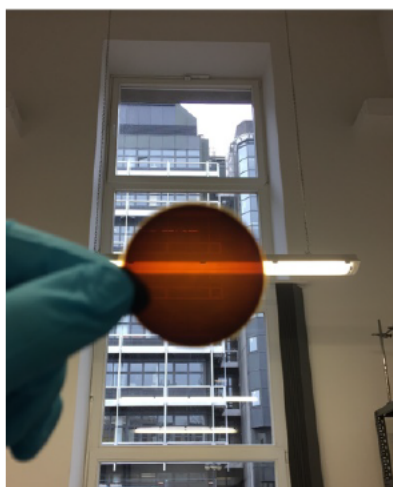
Figure 3.3 A Partially Transparent GO Folio

The prepared GO folio using this method has a thickness of 1-30 μm, and an average layer-to-layer distance of 0.83 nm (Dikin et al., 2007).

The prepared folio is then heated in 1100 °C under the protection of Nitrogen or Argon until most of the Oxygen functional groups are removed. After the last procedure, the electric conductivity is also restored.
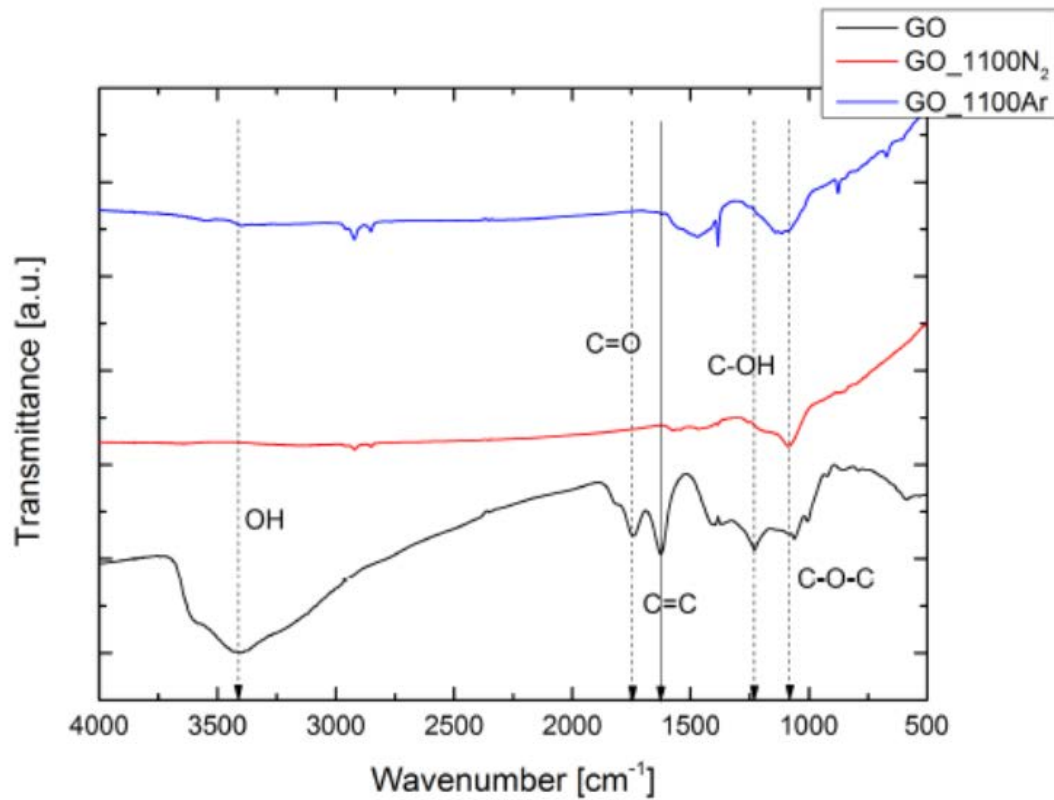

Figure 3.4 Remove of Oxygen Group

Since the reduction removes the oxygen groups and they leave the sandwich structure mostly in the form of gas, taking away 70% of the total mass, the sandwich structure may be therefore compromised. As a result, the r-GO folio loses most of its elasticity and becomes very fragile.
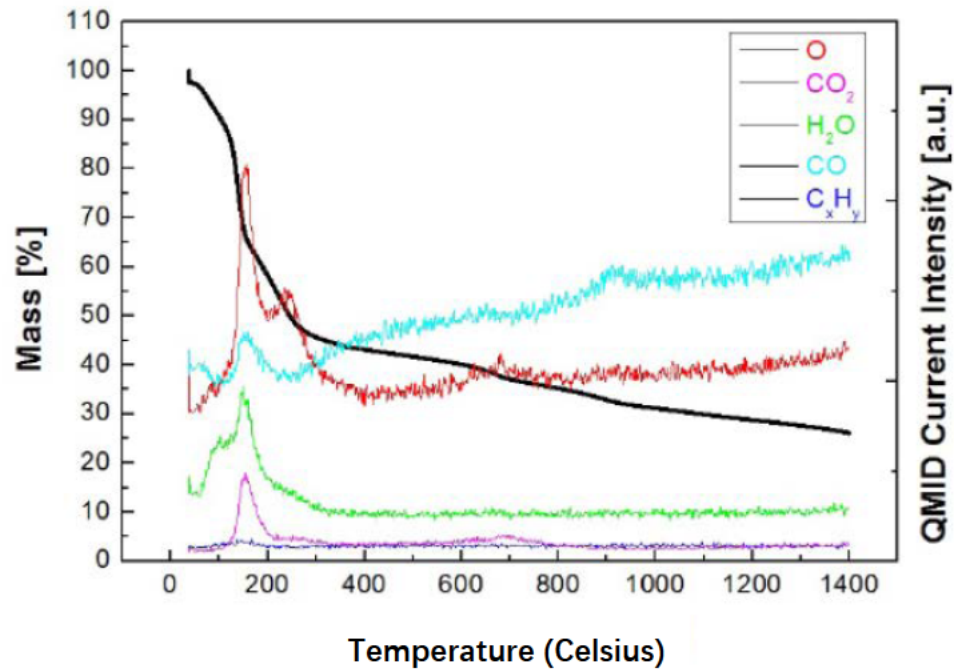
Figure 3.5 Loss of Mass during Heating (black line)

As for the r-GO folio mounted into DUTs, a further Scan Electron Microscope (SEM) on the cross-section reveals the layer-structure. The thickness of the folio can be controlled by the total mass of the GO flakes. An average thickness of approximate 2 μm and 10 μm are shown in following figures for samples using 3 mg and 13 mg mass of GO, respectively.
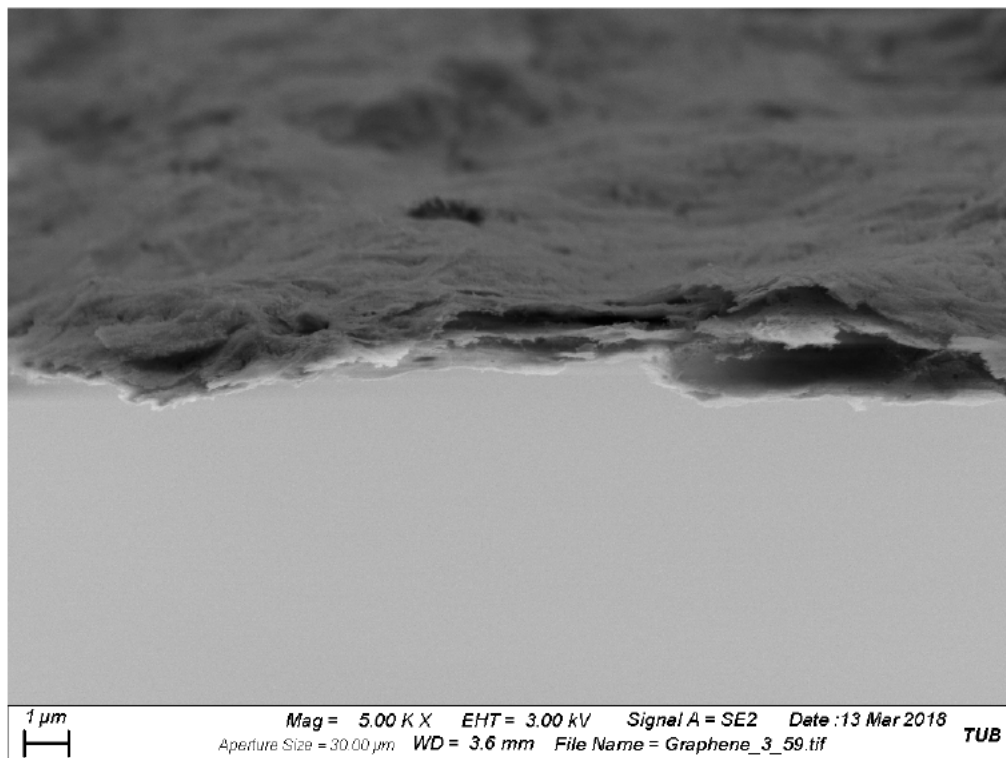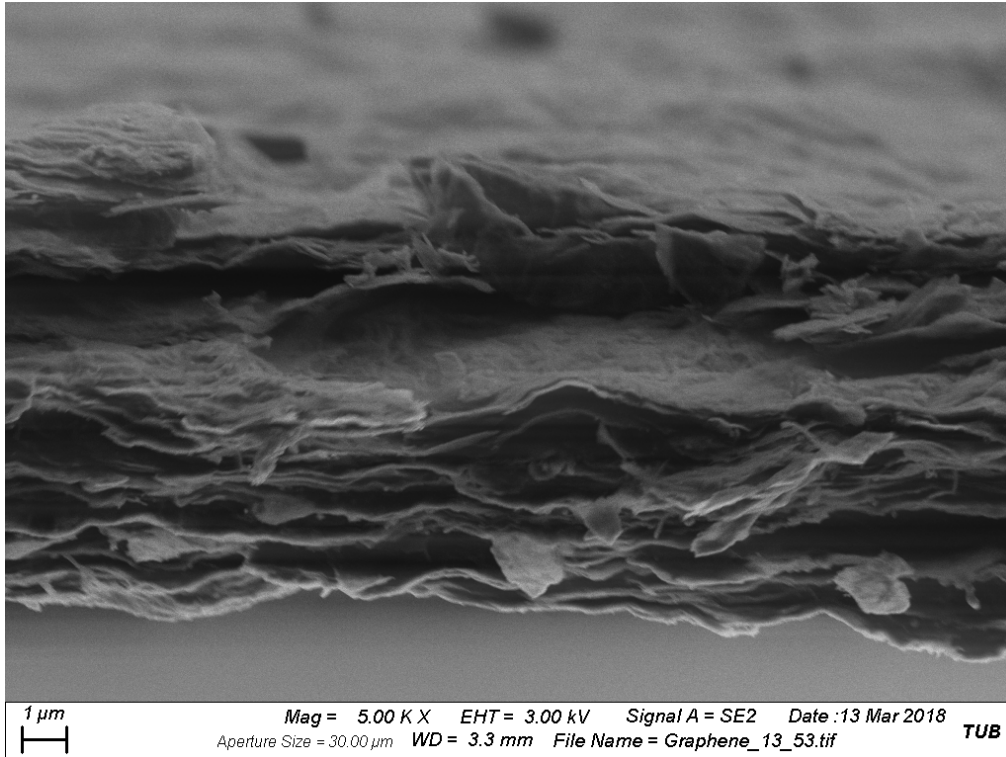

Figure 3.6 Cross-section of Folio under SEM, 3 mg GO

Figure 3.7 Cross-section of Folio under SEM, 13 mg GO

3.2. The Impedance of r-GO Folio

Although it was mentioned in some researches, that the CNT was tested to be pure resistive under MHz(Xiao et al., 2008) or below 10 kHz (Bouman, 2016) and theoretically, as the fundamental element of CNT, the graphene should also show similar electrical characteristics, we still cannot jump into the conclusion that the graphene folio we made is pure resistive, therefore an impedance measurement should be done to reveal the resistance and reactance of the folio. This is also very important for the properly choosing or even developing an amplifier which could drive the folio efficiently.

3.2.1. Theory

Among several practical methods of measuring the impedance, the easiest and yet still precise way of doing it is so called the "I-V method".

Since the impedance could be described as the "square root of the quadratic sum of the resistance and the reactance of the DUTs at different frequencies", which means for the impedance across the whole interested frequency band, one needs only to measure the voltage and the current accordingly of every frequency:

$$Z(f) = \frac{U(f)}{I(f)} \qquad\qquad (14)$$

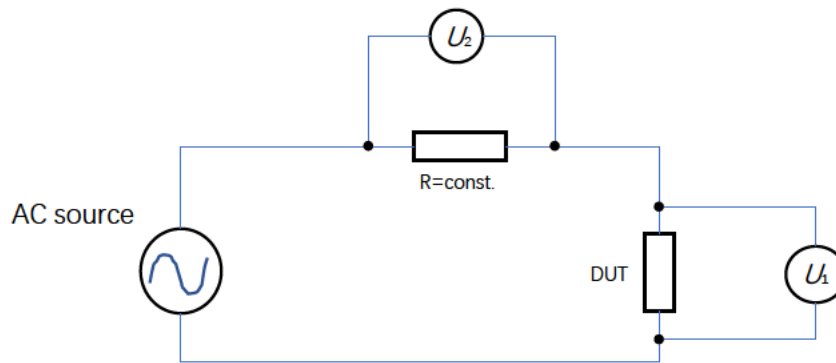A simple circuit could therefore easily be derived in Figure 3.8Figure 3.8 Theoretical

Figure 3.8 Theoretical Circuit for Impedance Test

Where:

R is a knowing resistance which at least one magnitude lower than the assumption impedance of the DUT

U_1 and U_2 are the measured voltage across DUT and R, accordingly. The internal Impedance of the test instruments should be significantly higher than the assumption impedance of the DUTs.

AC source delivers an excitation signal across the whole interested frequency band.

All the specifications of devices in practice could be found in Chapter 3.2.3

The impedance of the DUT could then be calculated:

$$Z(f) = \frac{U_1(f)}{I(f)} = \frac{U_1(f)}{U_2(f)} R \qquad (15)$$

3.2.2. Measuring setup

The actual setup is illustrated in Figure 3.9.
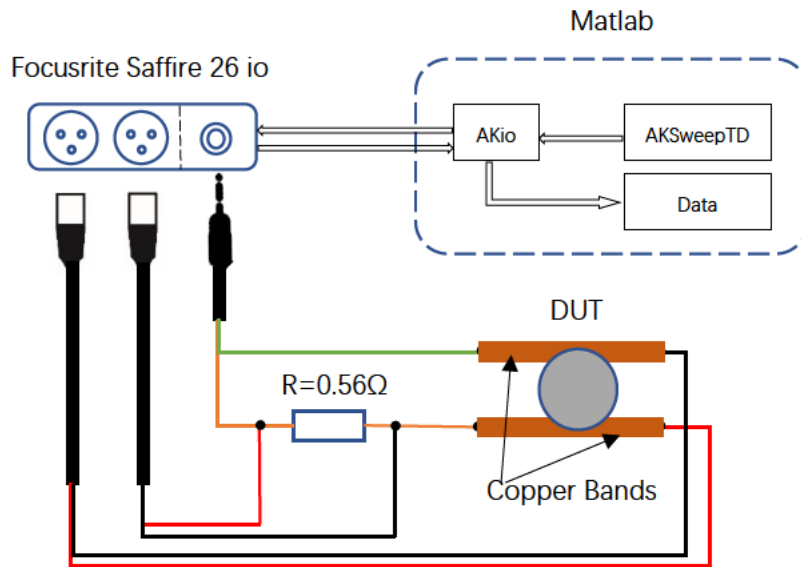
Figure 3.9 Impedance Test Setup

3.2.3. Instruments, software and DUT

   a. Focusrite Saffire 26 io

Firewire interface. The XLR Input 1 & 2 collect the voltage measured on DUT and R, accordingly. The setup and key specification of the interface are listed below:

- Sample rate: 48 kHz
- Input impedance: 2.5 kΩ
- Input frequency response: 20 Hz-20 kHz
- Equivalent Input Noise: >120 dB (60 dB Gain with 150 Ω termination)
- Output frequency response: 20 Hz-20 kHz
- Output Noise: -90 dBu

   b. Resistor R

A power resistor with 0.56 Ω characteristic Value. The actual value is measured before each test using a Multimeter.

   c. Pre-test speaker TF0818

A dynamic mid-range driver manufactured by Celestion, sealed in wood box. The key features are listed below:

- Nominal impedance: 8 Ω
- Frequency range: 70-6000 Hz
- Nominal diameter: 203 mm/8 inches
- Small signal parameters: Fs=95 Hz, Q_{ms}=3.83, Q_{es}=0.50, Re=6.4 Ω

More information about this driver can be found on its official website[2].

   d. Software

The MATLAB® (version: R2014a) and AK Tools(Brinkmann and Weinzierl, 2017) are

---

[2] https://celestion.com/product/110/tf0818/

used to generate a test signal and collect returning data from the sound interface.

The log sine chirp across 30 Hz-22050 Hz, lasts 10 seconds is chosen as the test signal. The sample rate is also 48 kHz, the same as the Sample rate of the sound interface. Since the Nyquist frequency of both sample rates is higher than the upper limit of the frequency response of Input & output channel, aliasing could be prevented. During the test for each sample, the signal will be repeated ten times consecutively. After each excitation, a Fast Fourier Transformation (FFT) will be executed to calculate the magnitude and phase. All the variables in the workspace will then be saved into separate files.

3.2.4. Process of Tests
1) Calibration

Since the output level is irrelevant to impedance measurement, the only factor that could affect the test result is the gain level of each input channel. To find out the precise gain factor in every setup, calibration is conducted as follows:

a. Loop the output directly back into input chn.1 & 2.

b. Set the gain of each input channel to almost the same scale around "5" to ensure enough SNR as well as avoiding potential overdrive.

c. Generate a sine Signal in MATLAB with the amplitude of 1 and frequency of 1 kHz, last 5 seconds.

d. Collect the signals from both input channels and save the amplitude as a gain factor for further use.

The Matlab® code could also be found in Appendix 2 Digital Data

The actual calculation of impedance should be slightly changed:

$$Z(f) = \frac{U_1(f)}{I(f)} = \frac{U_1(f)/G_1}{U_2(f)/G_2} R \qquad (16)$$

Where G_1 and G_2 are the gain factors of chn.1 & 2., respectively.

Note: this method is under the assumption that the gain factor is unified across all frequencies, all the frequency responses of the involved instrument, e.g., sound interface, will not be considered.

2) Pre-test with dynamic driver "Celestion© TF0818"

To make sure the whole setup works properly and meets the required precision, a pre-test with dynamic driver TF0818 is first conducted, whose acoustic and electric parameters are already given by the manufacturer.

There are two reasons for this pre-test:

a. The output voltage direct from the sound interface is not high enough to make folio producing any sound wave. A higher voltage could be achieved by using an amplifier, yet it will cause very high distortion in the input of the sound interface or even damage the input channel. Therefore, during the test, the folio is complete silence, the status of the system could not be heard.

b. By comparing the test result with the parameters given by manufacturer some errors of the setup could be noticed and corrected before the actual test.

3) Test for DUT samples

Each folio will first be mounted into a frame made of two pieces of hard cardboard. A window is carved out for the free hanging of the r-GO folio. With four M3 screws on each corner, the r-GO folio is pressed onto electrodes made of copper folio on both sides. This structure is to ensure a relatively consistent pressure between r-GO folio and electrodes so that the DC-resistance and impedance could remain stable.

A DC-resistance is then measured with a multimeter for further reference. After that, the test signal is fed to the folio, and the corresponding voltages are recorded. At last, the DC-resistance is once again measured with a multimeter.

3.2.5. Data Analysis

For each folio and the speaker, a mean value of impedance $Z(f)$ will be calculated using the data from 10 excitations. The raw data, as well as a smoothed curve, are demonstrated in the same figure.

a) Pre-test for Celestion© TF0818
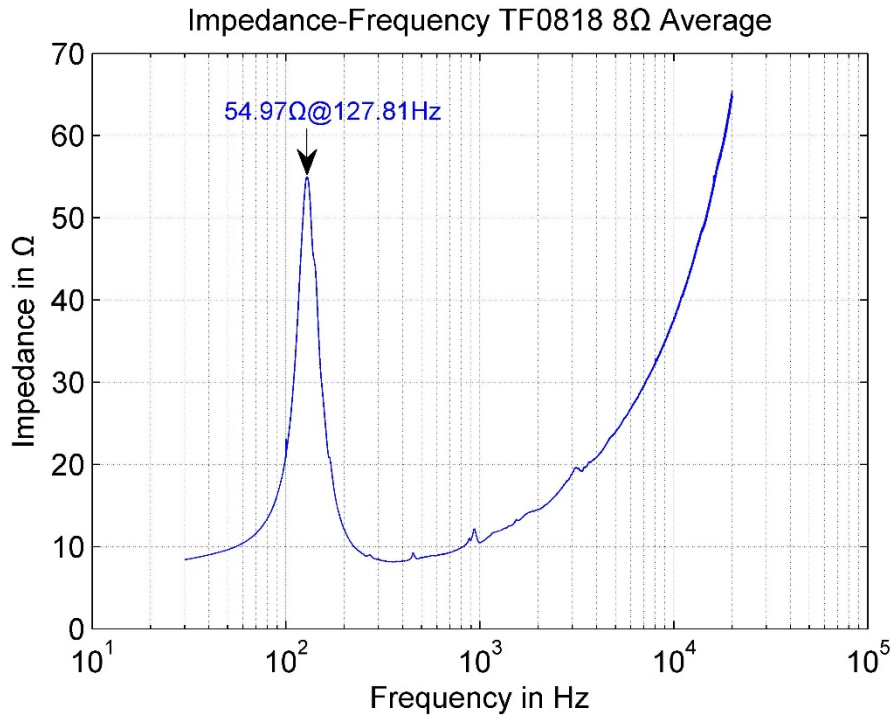
Figure 3.10 Impedance of TF0818

As shown in Figure 2.3, the measured maximal impedance reaches 54.97 Ω, at 127.81 Hz. Comparing with the theoretical value calculated from small signal parameters:

$$Z_{max} = Re \cdot \left(1 + \frac{Q_{ms}}{Q_{es}}\right) = 6.4\,\Omega \cdot \left(1 + \frac{3.83}{0.5}\right) = 55.42\,\Omega$$

The difference between measured value and the theoretical value is only 0.45 Ω (0.81%), which means the setup is plausible and meets the required accuracy.
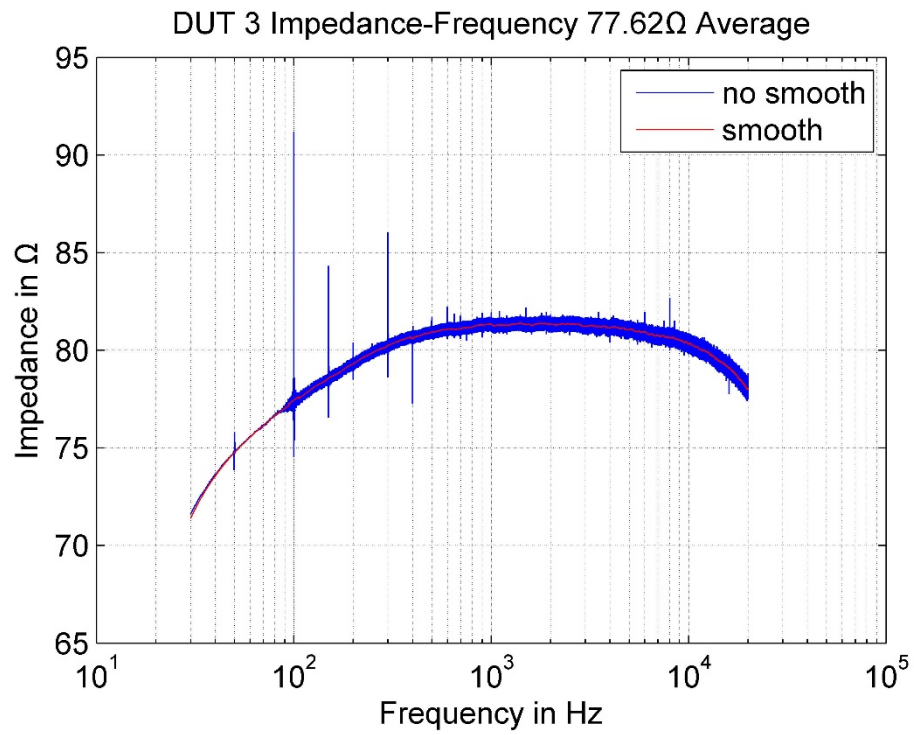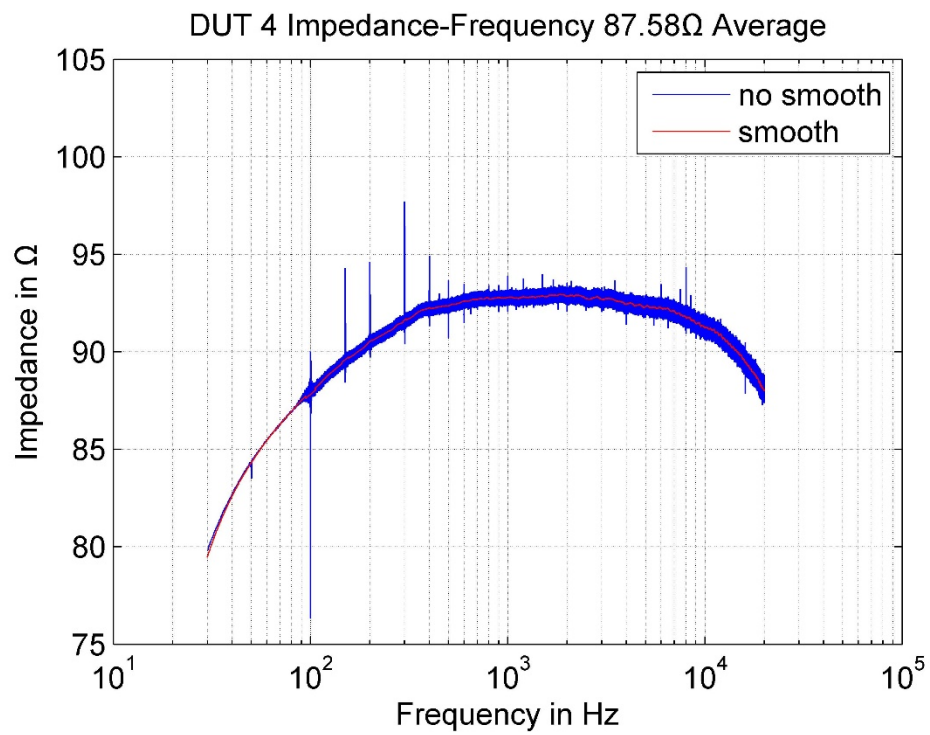
b) DUTs

DUT 1 Impedance-Frequency 17.57Ω Average

(a)

DUT 2 Impedance-Frequency 48.65Ω Average

(b)

DUT 3 Impedance-Frequency 77.62Ω Average

(c)

DUT 4 Impedance-Frequency 87.58Ω Average
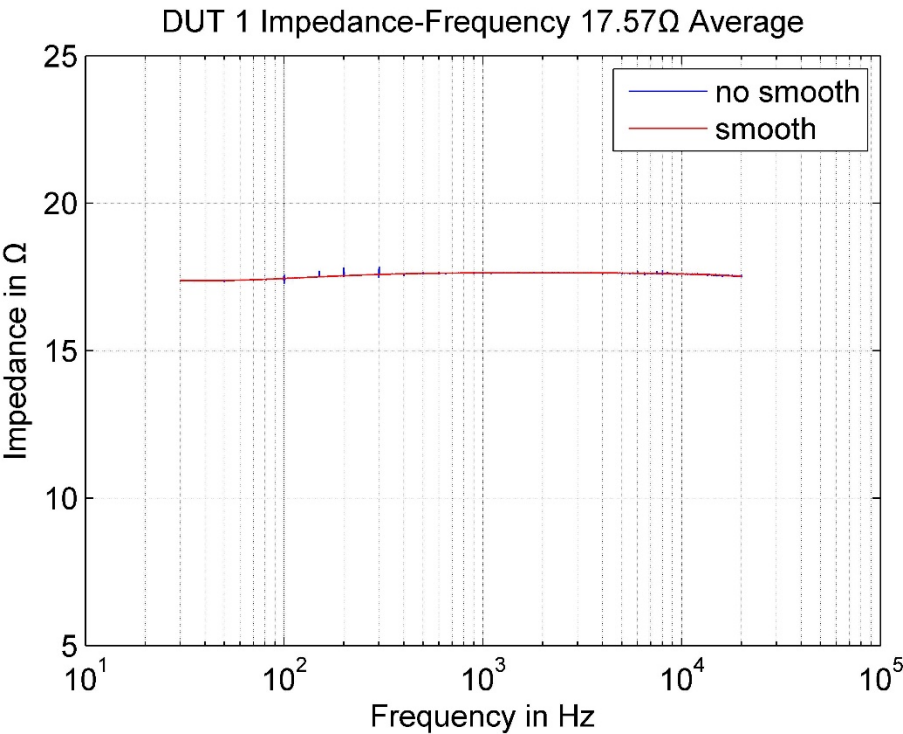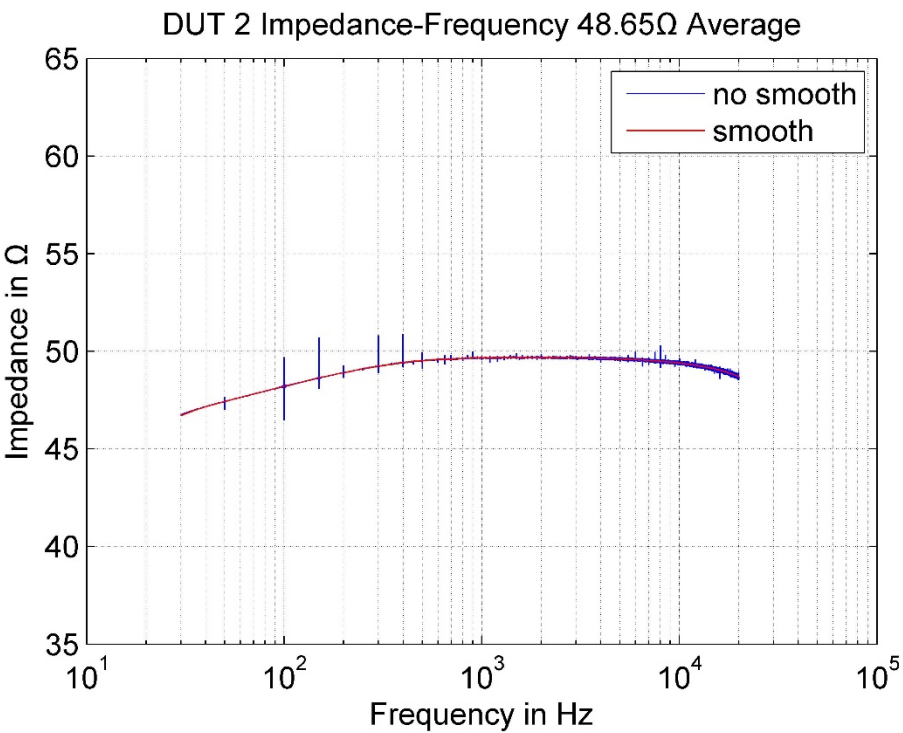
(d)

Figure 3.11 Impedance-Frequency of 4 DUTs.

For better visualization, the original data is smoothed with moving average method calculated with a filter coefficient of 0.008, showing in the red line.

The impedance of 4 DUT shows a very different trend comparing with the electrodynamic transducer. The impedance is reversed proportional to the frequency with a narrow steady part between 1 kHz and 6 kHz, suggesting that a flat frequency response may be found in this frequency band. However, since the density of different parts of the folio is not uniform, even different parts of the same folio (i.e., DUT1 & DUT2) show different electric characteristics. The impedance is also influenced by the pressure applied which presses folio on the copper bands.
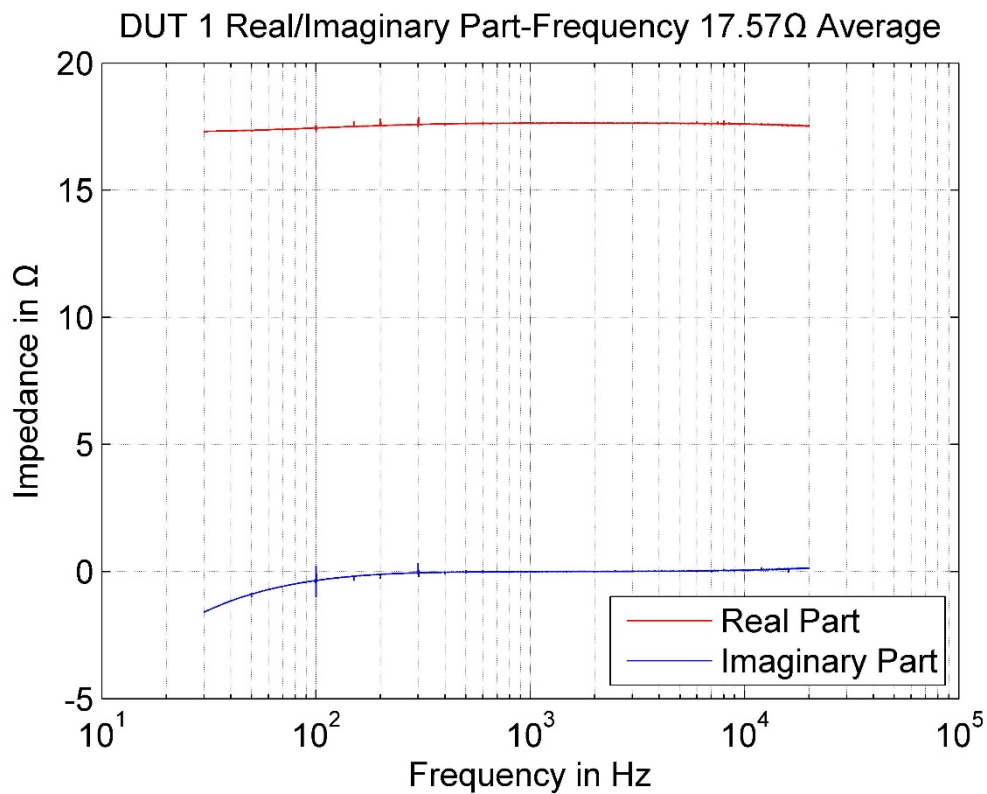
(a)
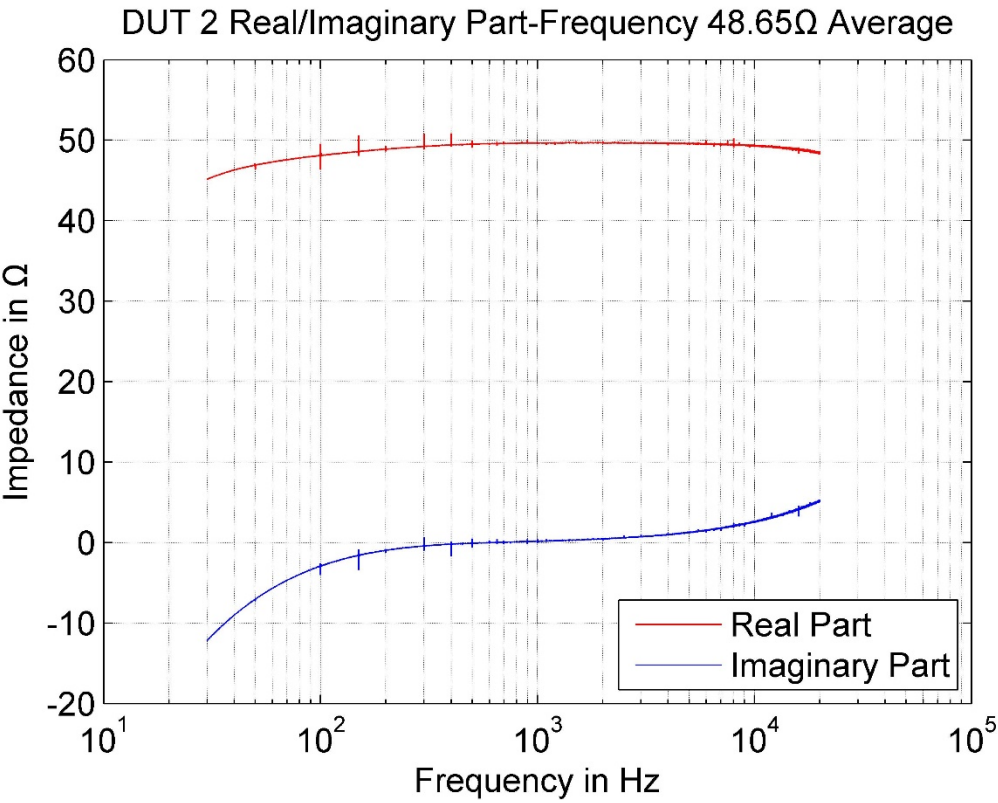
(b)
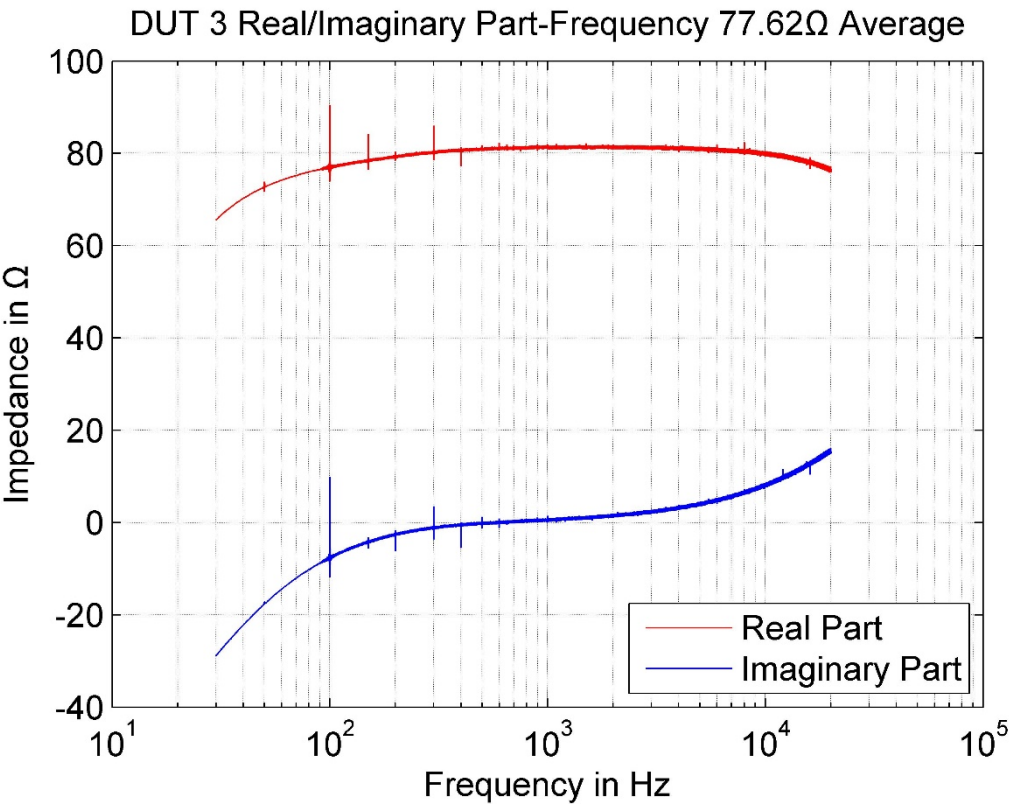
(c)
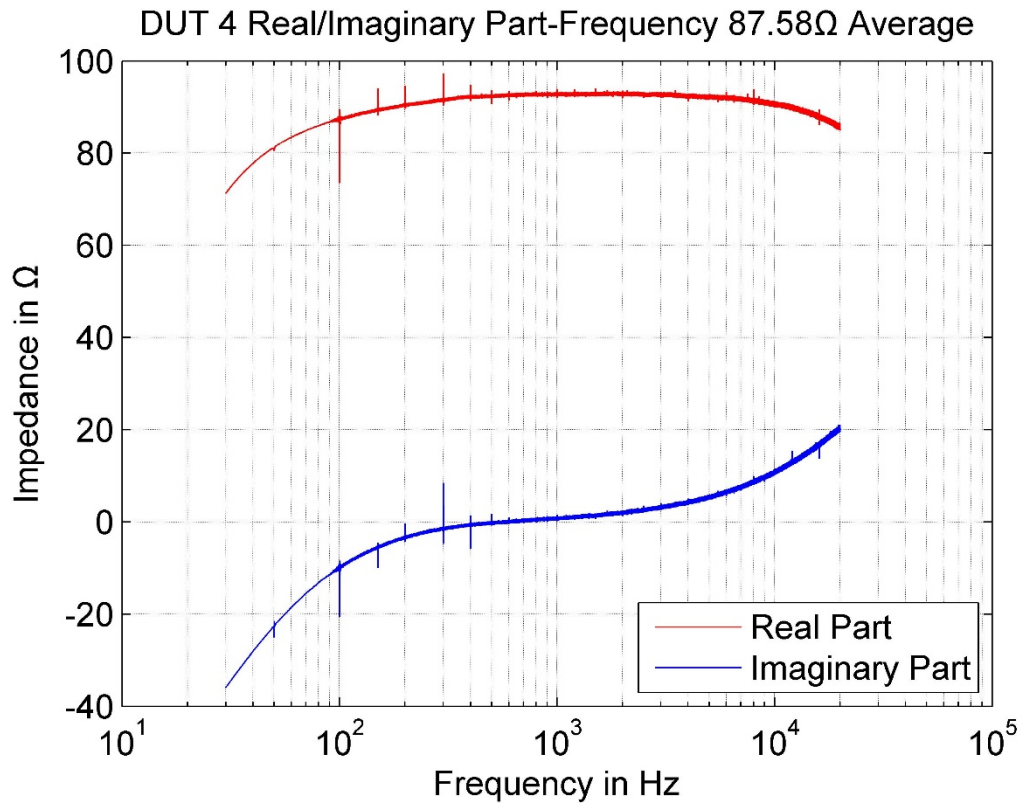
(d)
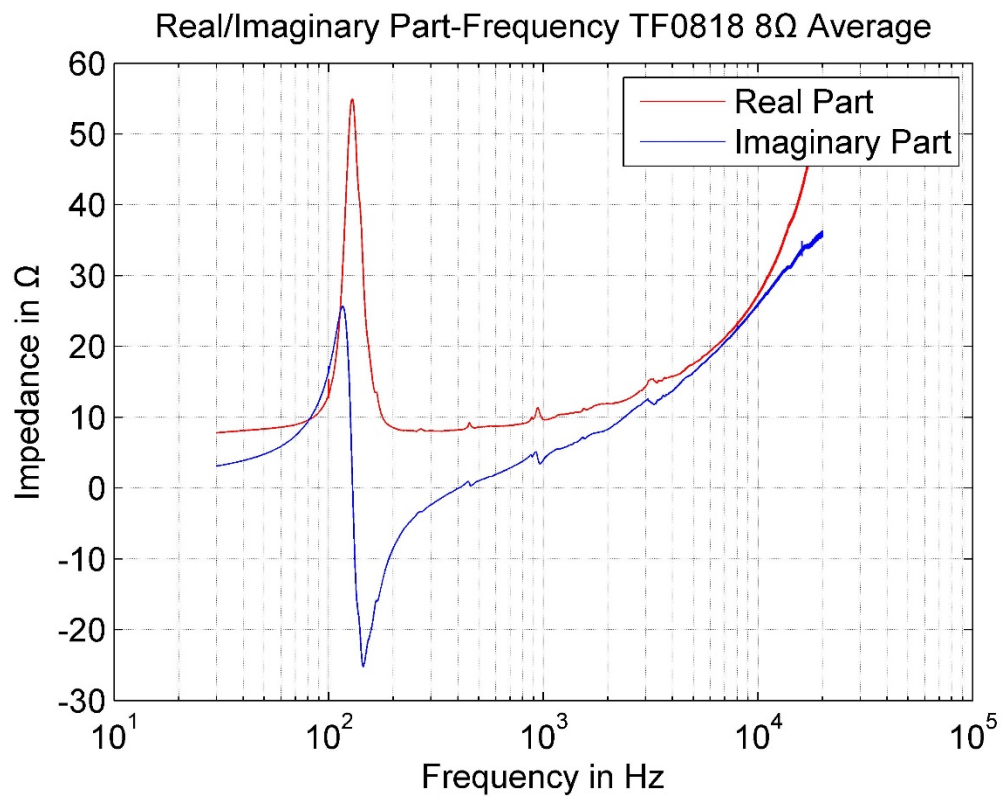
(e)

Figure 3.12 Real/Imaginary Part of Impedance. (a) –(d): DUT1~DUT4; (e) Electrodynamic Driver

From Figure 3.12 the characteristic of the folio can be distinguished from the dynamic speaker. Depending on the average density, the folios show slight different characteristics, especially when the frequency under 100 Hz and over 5 kHz. Nevertheless, compared to the dynamic speaker, the folio should be considered as an almost pure resistive material in the frequency band of 250 Hz-16 kHz.
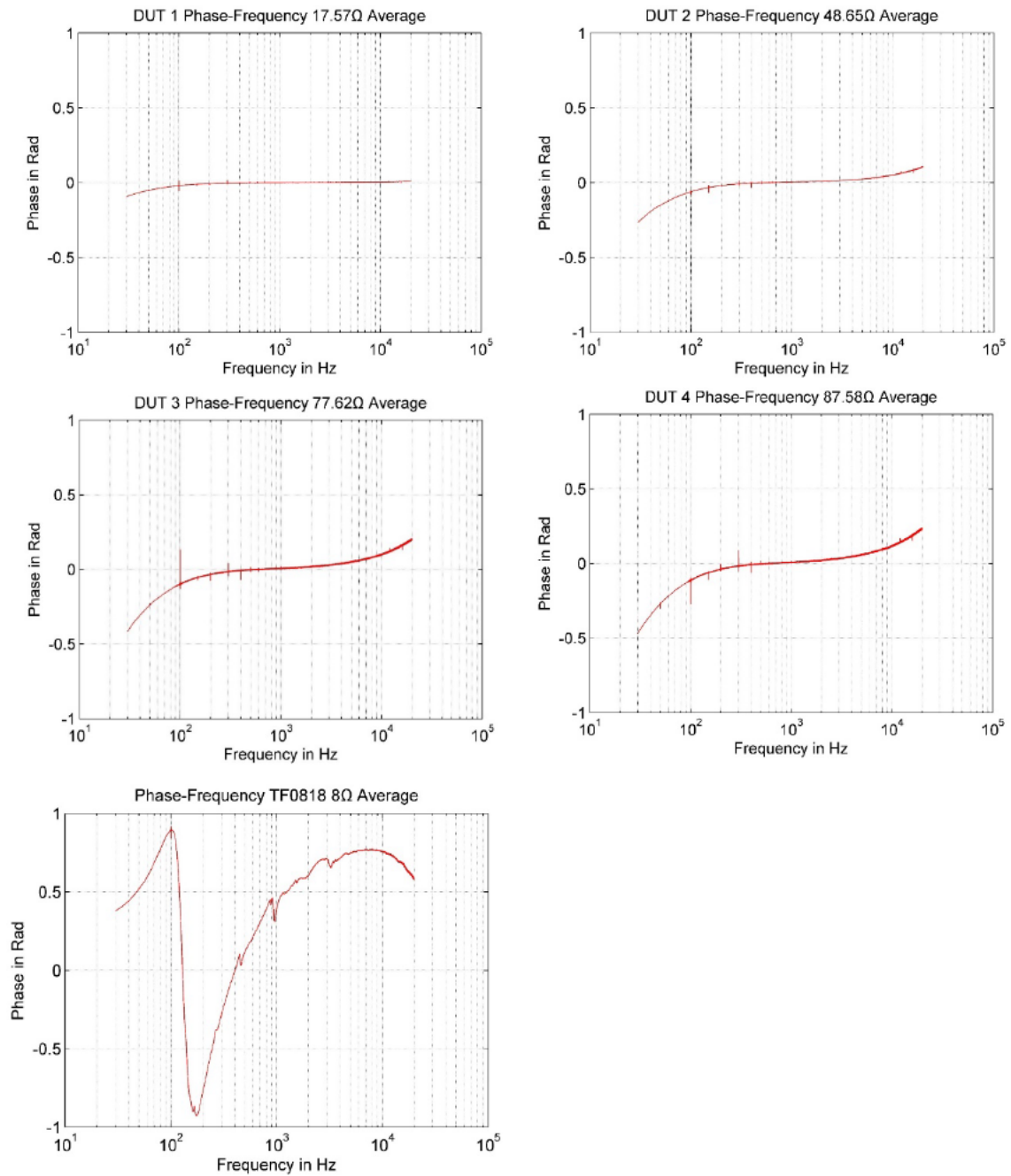
Figure 3.13 Phase of Impedance

The phase of impedance also confirms the different characteristics between the folio and dynamic speakers. While the phase of dynamic speaker shows apparent reactive trait, the phases of folios are all flat and almost constant at zero from 250 Hz to 5k Hz, indicating that within this frequency band the folio consists mostly resistive component.

4. Prototypes of Driving Circuit

As above mentioned, there are several ways with which the correct signal could be reconstructed. However, the most straightforward way is definitive DC-Offset. This is quite unordinary since for, i.e., electrodynamic transducer any DC-Offset should be avoided and at the output of almost all amplifier for this purpose, there is a high-value capacitor which decouples any DC component from any stage of signal chain so that the transducer would not be jeopardized. Therefore, to introduce DC-Offset into the signal again, the auxiliary circuit is needed.

4.1. Prototype 1: DC Couple with Accumulator

At the early stage of this research, a simple solution was considered as in Figure 4.1:
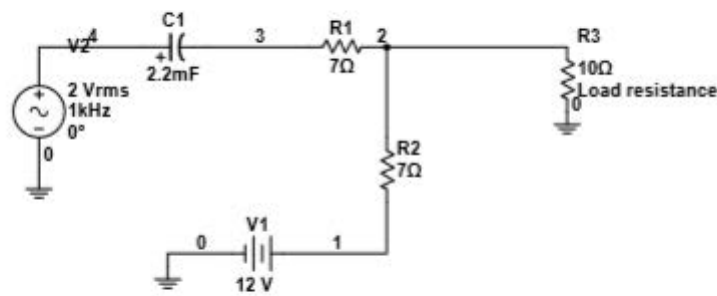
Figure 4.1 Accumulator Circuit

The advantage of this circuit is obvious, only several resistors and capacitor are needed. It was quite useful for quick verification of the theory of thermoacoustic. However, since the current needed is quite strong, all the resistors must be power resistors and yet be heated dramatically while driving the folio, the potential stability is in question. Another disadvantage of it could be the level of coupled DC voltage. It solely depends on the voltage of accumulator and could not be easily adjusted manually.

4.2. Prototype 2: OPA Circuit with Adjustable DC-offset

Another circuit utilizing Operation Amplifier (OPA) has been built later proving a better heat dispersion as well as adjustable DC-Offset, as shown in Figure 4.2.
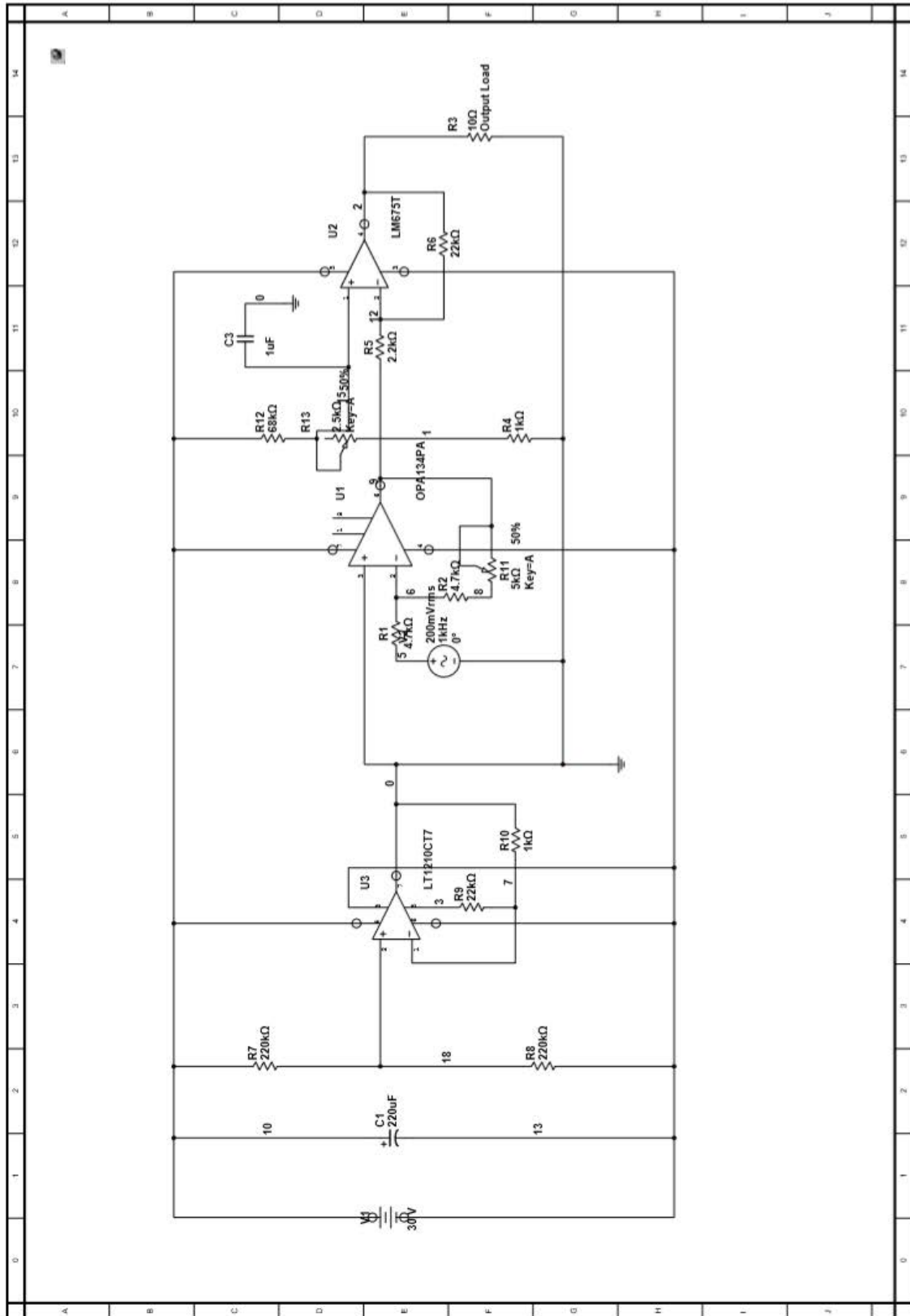
Figure 4.2 OPV Circuit

All OPA are in TO-220 package; suitable heat sinker could easily be mounted on the surface of the IC to achieve better heat dispersion and avoid protective shut down of IC. The selected heat sinker for LT1210 and LM675 can provide 5K/W thermal resistance.

By adjusting the potential meter R11 and R13, different ratios of signal and coupled DC voltage could be set.

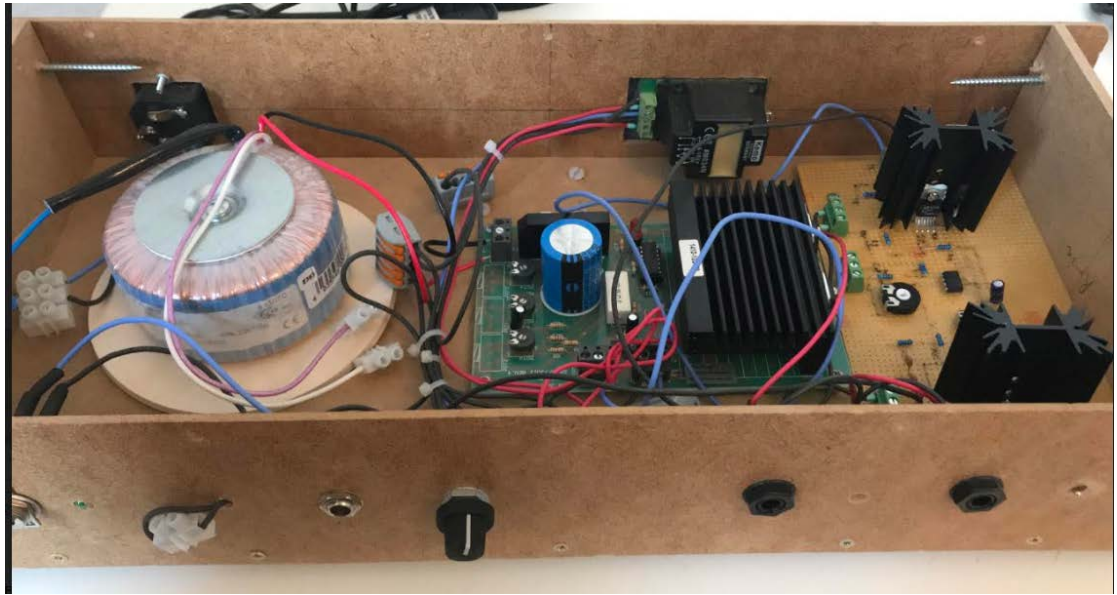All other periphery devices including power supply are mounted into a wooden case as showed in Figure 4.3

Figure 4.3 Overview of Device

5. Electroacoustic Efficiency

5.1. Theory and Concept

5.1.1. Definition of Electroacoustic Efficiency

The acoustic efficiency can be experimentally evaluated as follow:

$$\eta = \frac{P_A}{P_E} \times 100\% \tag{17}$$

Where

P_A: acoustic power

P_E: electric power consumed by the transducer

5.1.2. Electric Power

The electric power can be calculated by:

$$P_{E,RMS} = U_{RMS} I_{RMS}$$

Since the folio can be treated as pure resistive, the average electric power consumed by folio can be then expressed using the resistance of folio:

$$P_{E,RMS} = \frac{U_{RMS}^2}{R} \tag{18}$$

alternatively, for sine signal:

$$P_{E,RMS} = \frac{\widehat{U}^2}{\sqrt{2}R} \tag{19}$$

where

U_{RMS}, I_{RMS}: the effective value of voltage and current, respectively

R: \qquad resistance of DUT

$\widehat{U}$: \qquad amplitude of sine signal

5.1.3. Acoustic Power

Theoretically, there are two methods to determine the acoustic power of a sound source.

The first method utilizes the echo chamber. The critical problem in our situation is, the energy delivered by the transducer is too low to fill an echo chamber (typically approximate 200 m3), making this method nearly impossible.

The second method utilizes on the other hand anechoic chamber, by measuring the sound pressure in different points enveloping the sound source, the sound intensity level can be directly yielded:

$$L_I = 10\log\frac{|\vec{I}|}{I_0} = 10\log\frac{\tilde{p}^2}{p_0^2} = L_p \tag{20}$$

The acoustic power can be calculated:

$$P_A = \int I dS \qquad (21)$$

Alternatively, for a quasi-point source with spherical radiation in an anechoic chamber, it can be further simplified:

$$P_A = I \times 4\pi r^2 \qquad (22)$$

For a quasi-point source sitting on a hard-reflective surface, the envelope surface should then be hemispherical, and the acoustic power can be calculated as:

$$P_A = I \times 2\pi r^2 \qquad (23)$$

where r is the distance between the microphone and sound source.

More specific for the folio, the reflection from the environment is not crucial since the emitted SPL is approximate 30 dB to 50 dB at about 3 cm distance. On the other hands, however, the background noise level of environment could significantly affect the measured SPL and must be limited as low as possible. The anechoic chamber is therefore still the best choice for the measuring of sound power. According to DIN EN ISO 3744   (DIN, 2010), the average sound power should be calculated using the measured SPL of several points on a hemisphere surface.
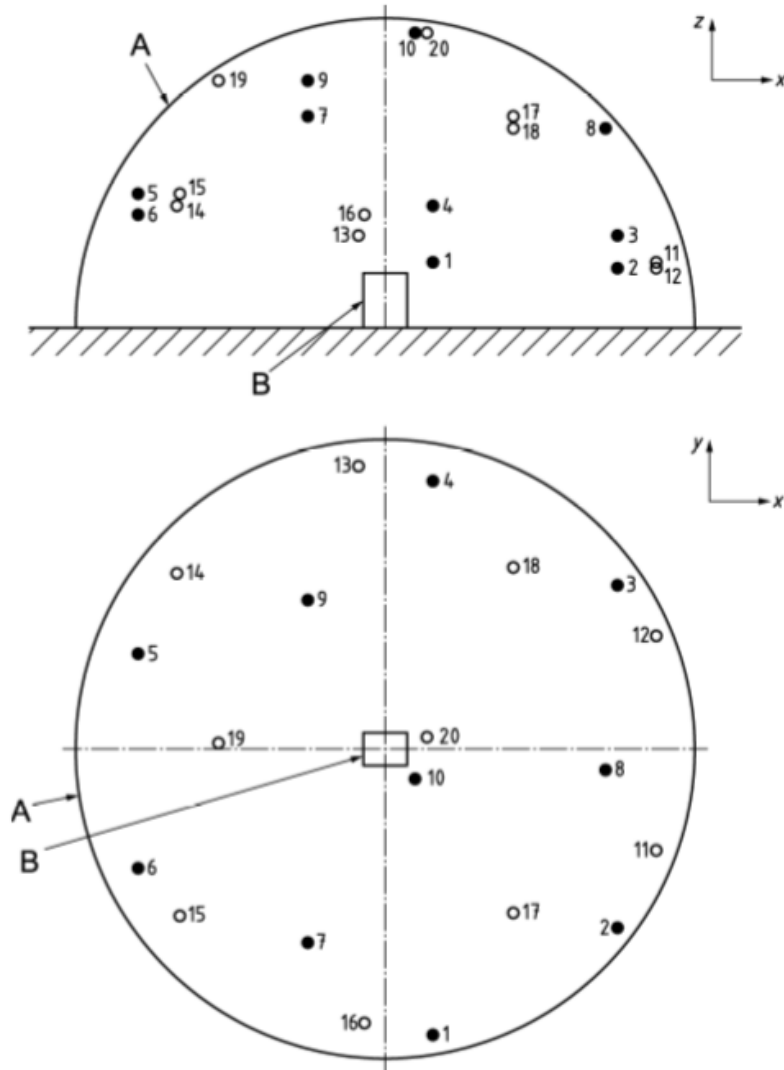
Legende

● Hauptmikrofonpositionen (1, 2, 3, 4, 5, 6, 7, 8, 9, 10)
○ zusätzliche Mikrofonpositionen (11, 12, 13, 14, 15, 16, 17, 18, 19, 20)
A Messfläche
B Bezugsquader

Figure 5.1 Microphone Positions on Hemisphere (DIN, 2010)

In practice, the radius of the hemisphere could not be big enough to contain so many microphone positions, and under the assumption that the emission of sound pressure is symmetric on both sides of the folio, seven measure points on the hemisphere in front side are randomly selected for each DUT.

The average SPL can be then calculated as follows:

$$\overline{L_p} = 10\lg[\frac{1}{N_M}\sum_1^{N_M} 10^{0.1L'_{pi}}] \tag{24}$$

where

L'_{pi}: time averaged sound pressure level of the i-th microphone position in dB

N_M: number of microphone position

The Sound power level is then given:

$$L_w = \overline{L_p} + 10\lg\frac{S}{S_0} \text{ dB} \tag{25}$$

where

S: the surface area of the envelope hemisphere in square meter

S_0: 1 m^2

And finally, the sound power:

$$P_A = P_0 \cdot 10^{0.1L_w} \tag{26}$$

where

$P_0 = 10^{-12}$ W, the reference value of sound power

5.2. Test Setup

The test was conducted on February 22nd, 2018 in the anechoic chamber in "Prüfhalle" of TU-Berlin. The setup is summarized in Figure 5.2
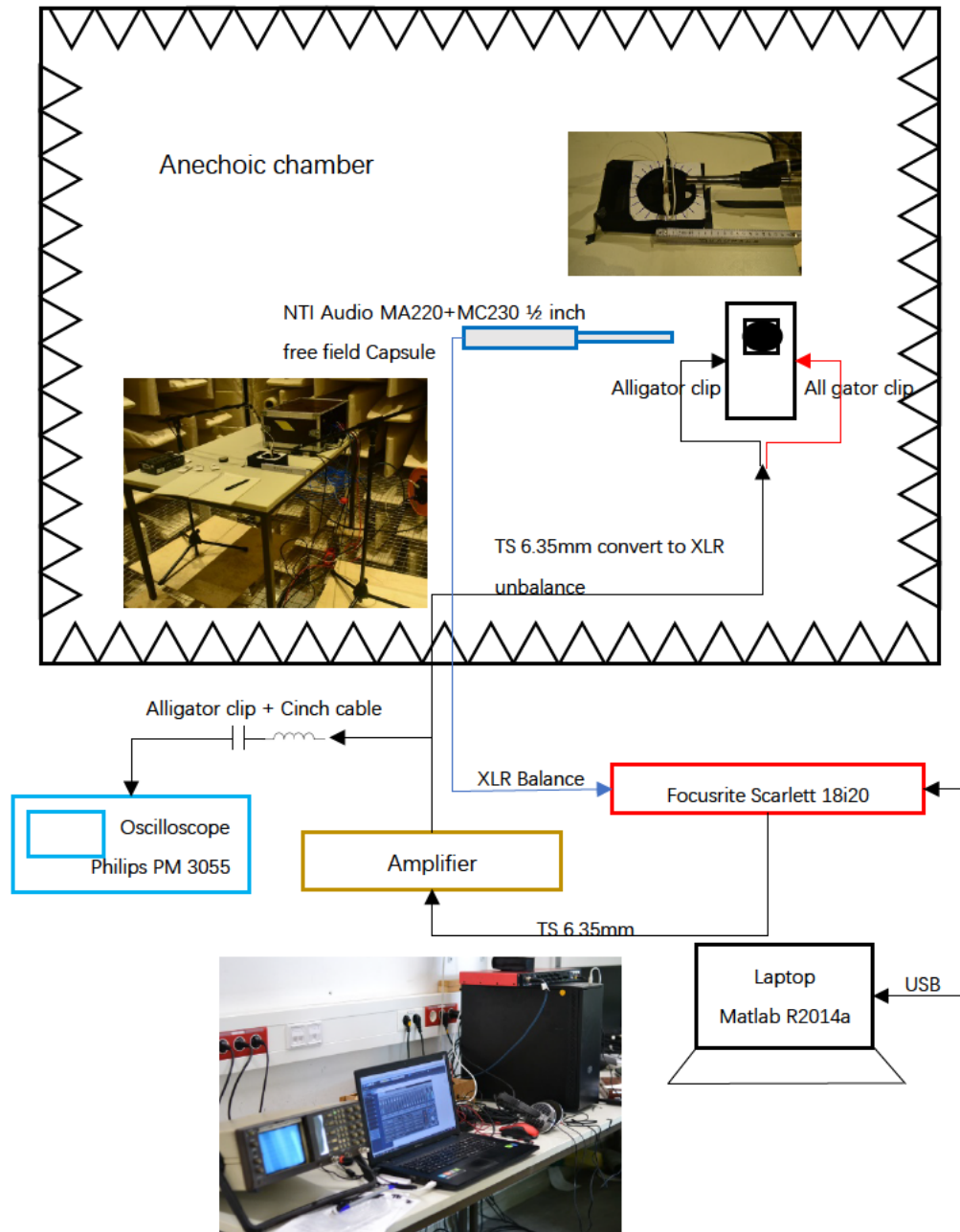
Figure 5.2 Setup of Primary Test

5.2.1.   Technical Specifications

    a)   Anechoic Chamber[3]

        Volume ： 1070 m^3

        Walkable area: 126 m^2

        Lower frequency limit: 63 Hz

    b)   Sound Interface[4]

- Focusrite Scarlett 18i20 1st Generation
- Driver version 1.19 beta12 for Windows 10
- Sample rate: 48 kHz
- Microphone Inputs

    Frequency Response: 20 Hz ± 0.5 dB, 20 kHz ± 0.1 dB (min. gain)

    THD+N: 0.001% (1 kHz, –1dBFS, 20 kHz BW)

    Noise EIN: –122 dBu CCIR-RMS (measured at 60 dB of gain with

                         150 Ohm termination)

    Maximum input level: +8 dBu (without pad)

- Line Outputs 1 & 2

    Maximum Output Level (0 dBFS):   +16 dBu, balanced

    THD+N ：   0.001% (1 kHz, –1dBFS, 20 kHz BW)

    c)   Amplifier

        see Chapter 4.2

    d)   Oscilloscope[5]

- Philips PM 3055
- Analog Oscilloscope
- Bandwidth for 20 mV to 10V: >60 MHz
- Deflection coefficient: 2 mV/div to 10V/div
- Max. input voltage: 400 V (dc + ac peak)
- Time coefficient: 0.5 s to 50 ns in Main Time Base (MTB) mode

    e)   Microphone[6]

- NTI Audio M2230 Class 1 certificated
- ½ inch free field capsule MC 230 (Removable)
- Pre-amplifier MA220
- sensitivity: 42 mV/Pa @ 1 kHz
- Frequency response: 5 Hz- 20 kHz

---

[3] http://www.akustik.tu-berlin.de/fileadmin/fg23/Sonstiges/Technische_Einrichtungen/Anechoic_Room.pdf

[4] https://d2zjg0qo565n2.cloudfront.net/sites/default/files/focusrite/downloads/8424/scarlett18i20-user-guideeng.pdf

[5] http://www.helmut-singer.de/pdf/phpm3050_pm3055.pdf

[6] http://www.nti-audio.com/Portals/0/data/de/Messmikrofone-Spezifikationen.pdf

f) DUTs

DUT ID	Density[7] in mg/cm^3	The valid area in cm^2	Thickness in μm	DC-Resistance in Ω	
1	418.52	2.25 cm^2 (1.5 cm×1.5cm)	2	83	
2	418.52	Approx. 2 cm^2 (2 cm×2 cm/2)	2	62	
3	362.72	Approx. 4 cm^2 (2 cm×2 cm)	10	450	
4	362.72	Approx. 4 cm^2 (2 cm×2 cm)	10	97	

Table 1 Features of DUTs

---

[7] Calculated using the 30% mass of GO, see Chapter 3.1

5.2.2. Test Procedure

i. Connect all equipment using specific cables as shown in Figure 5.2. Disconnect temporally DUTs from the system, send a test signal of 1 kHz from Laptop, adjust the signal amplitude and DC-offset of the amplifier by visually observation on an oscilloscope, avoiding any clipping or distortion. Final AC amplitude and DC level are set at 3.2 V and 4 V, respectively.

ii. Calibrate test microphone. Turn on CAL 200 calibrator which can calibrate the microphone to 94 dB SPL @ 1 kHz. Run program "calibrateMic" based on Matlab and the measured calibration factor is save for further usage. Several tries may be needed to maximize the microphone gain of sound interface yet not introduce any clipping or distortion.

iii. Connect DUTs back into the system and send test signal again, observe the oscilloscope for any anomalous. Check the AC and DC level.

iv. set up the test platform in an anechoic chamber. Adjust the distance between microphone front end and the center of foam base to 3 cm. Fix each corner of the foam base with adhesive tape on the table.
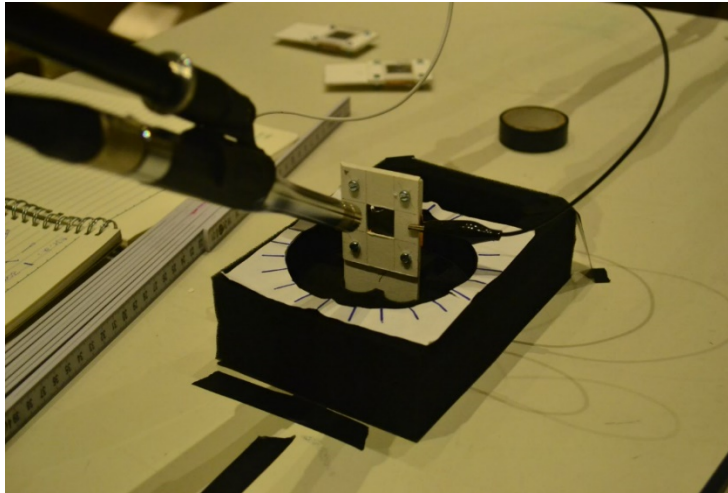

Figure 5.3 Foam Base Setup

v. Insert DUT into the foam base. Adjust the height of microphone to on-axis position and recheck the distance of 3 cm. Remove the protection sheets and connect the alligators to both electrodes.
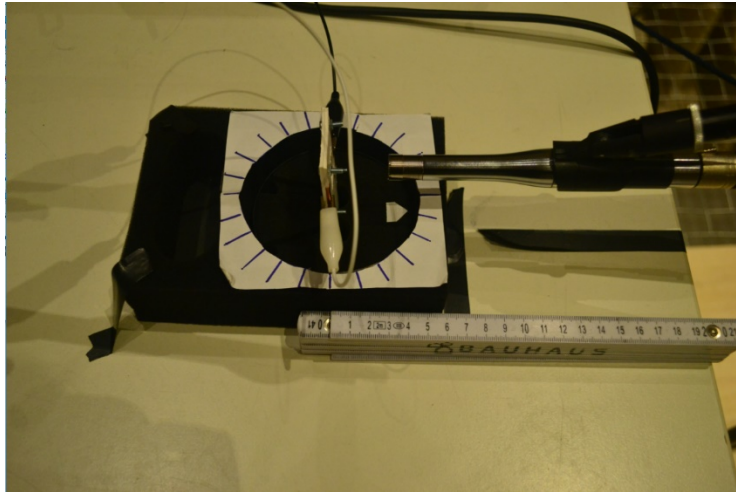
Figure 5.4 Microphone on-axis

vi. Seal the door of the anechoic chamber. Monitor the input from the microphone with a headphone to make sure the vibration of the net-floor and other accessories already fade out.

vii. Run program "SchallleistungMessung". Input the number of position, duration of the test signal and the ID number of DUT.

viii. Follow the instructions for each frequency at each position. During the excitation, adjust the scale of the oscilloscope and read for AC amplitude as well as take a photo for each excitation. After the excitation, input current amplitude and DC level (check after excitation to make sure it remains on 4 V). Input "0" for both AC and DC if a repeat is needed for current frequency.
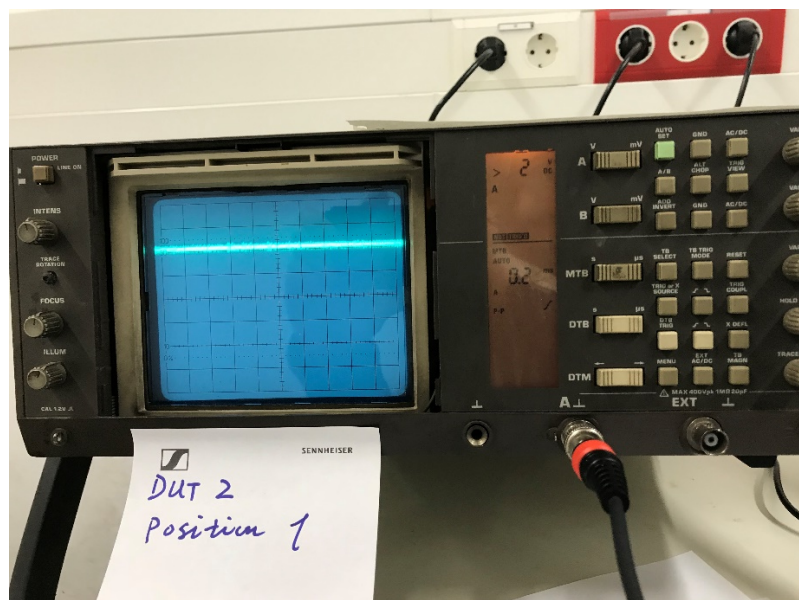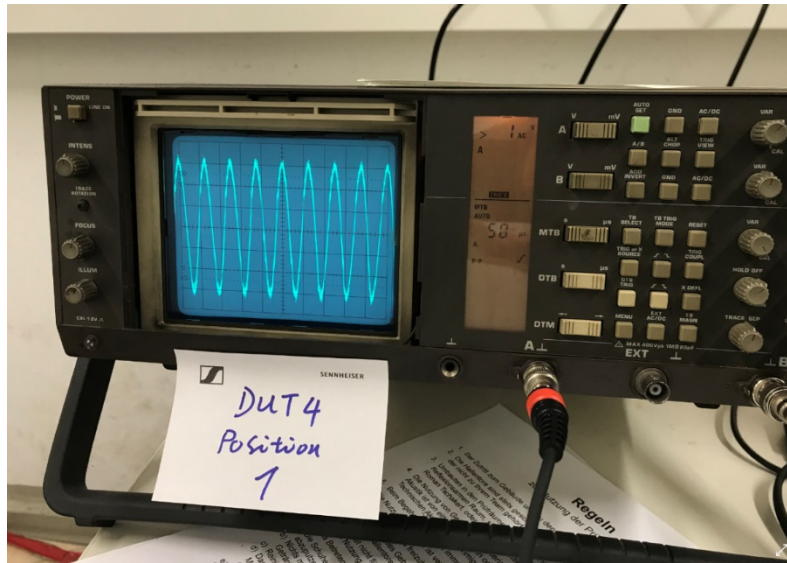

Figure 5.5 Check the DC Level

Figure 5.6 Monitoring the AC Level

    ix.   After seven times excitations for one position, the program will pause. Turn the DUT to another angle or rise the microphone height for the new position. Recheck the distance between microphone front end and center of the DUT after each movement.
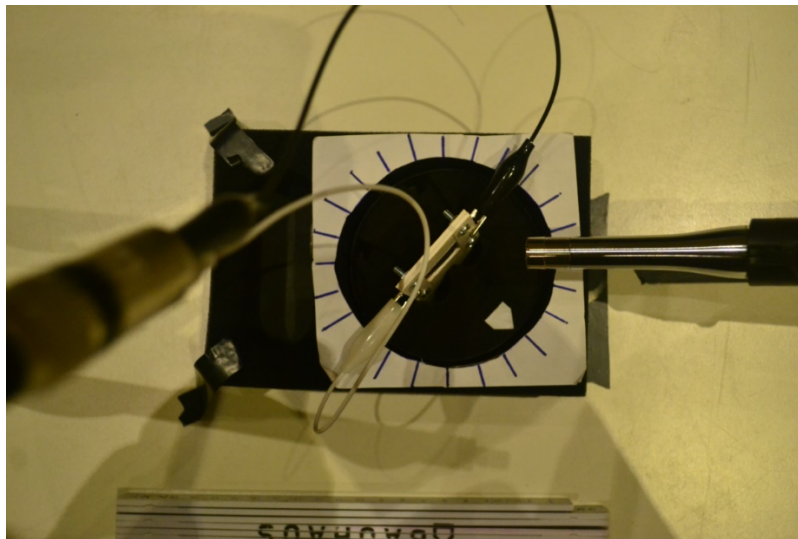

Figure 5.7 Turn DUT to Next Angle

    x.   Follow the instruction until all seven positions are done.

    xi.   Save the data. Program ends

    xii.   Repeat step vi. to xii. until 4 DUTs are tested.

Note:

To find out a proper combination of AC and DC voltage, some pre-tests have already been done previous the formal test. The upper limit of the voltage (DC plus AC peak) should be around 10 V due to the accumulation of heat which will eventually incinerate the folio, as shown in figure 31.

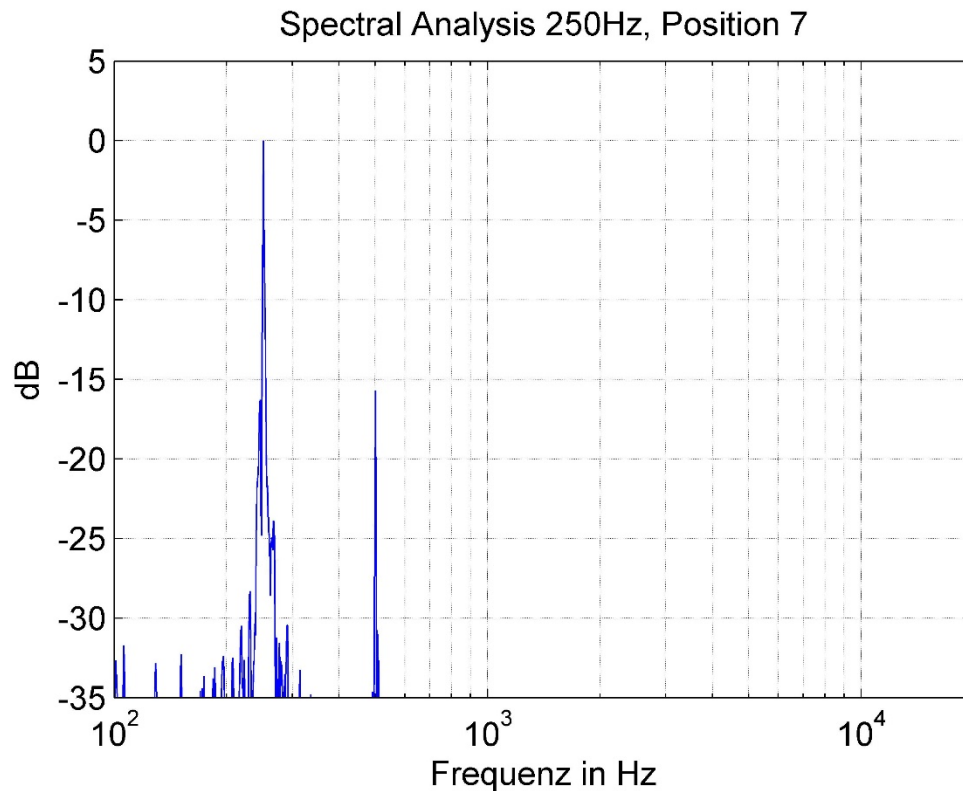Figure 5.8 A Burnt Through Folio, Test Voltage approx. 12 V Peak

Although the amplifier is designed to provide maximal ±14 V driving voltage giving 30 V supply voltage (non-rail-to-rail OPA), for the sake of the integrity of the folio, lower than 8 V should be the safe region. On the other hands for a lower 2nd- harmonic distortion, an optimal ratio of DC and AC should be 1 or more. Finally, to lower the heat due to DC part of the electric power (see Eq. (5)), a higher AC rather than DC level should be more appropriate. Ideally, the combination of AC=4 V and DC=4 V should, therefore, be the best solution. In practice, a combination of AC 3.2V peak and DC 4V has been chosen to gain a little bit more safety buffer to the upper limit.
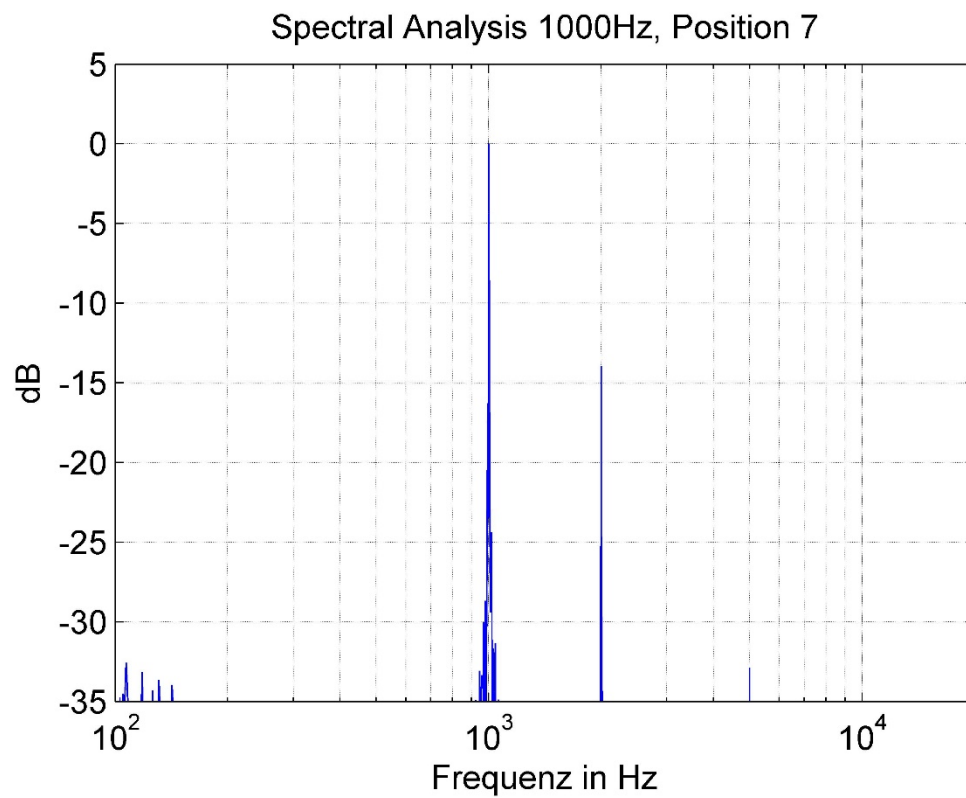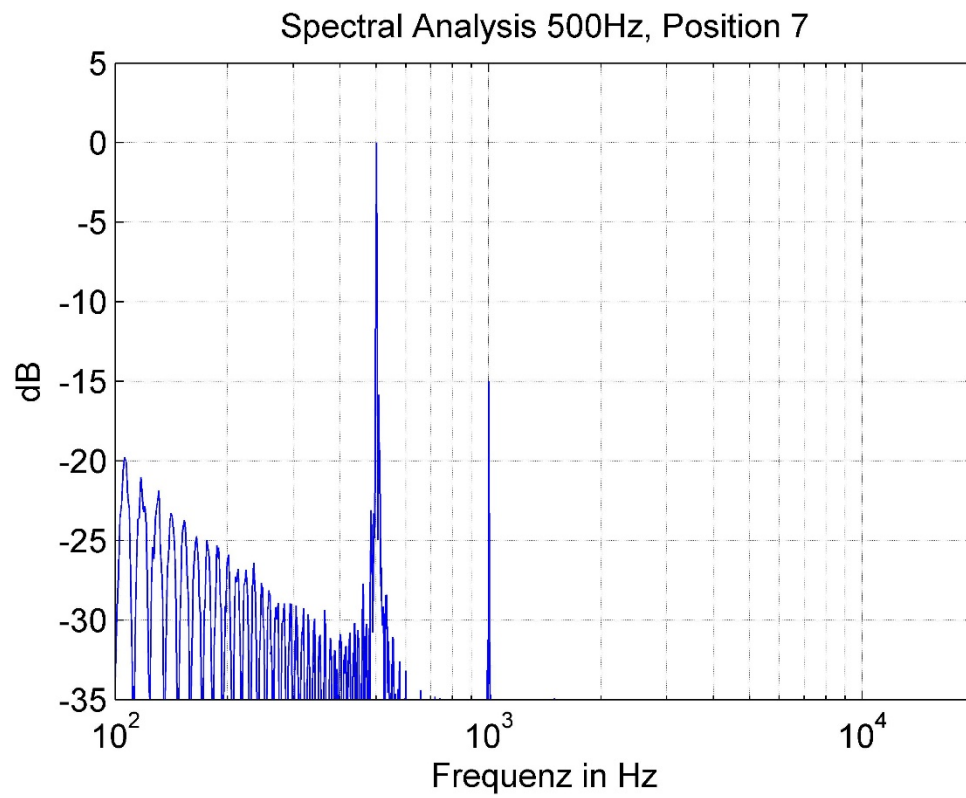
5.3. Result

4 DUTs have been measured for seven frequencies in octave band on seven positions. Despite the precautions, DUT1 has not survived through the whole process, entirely breaking into two halves after first two excitations on position 6 and therefore only five positions have been evaluated for it.
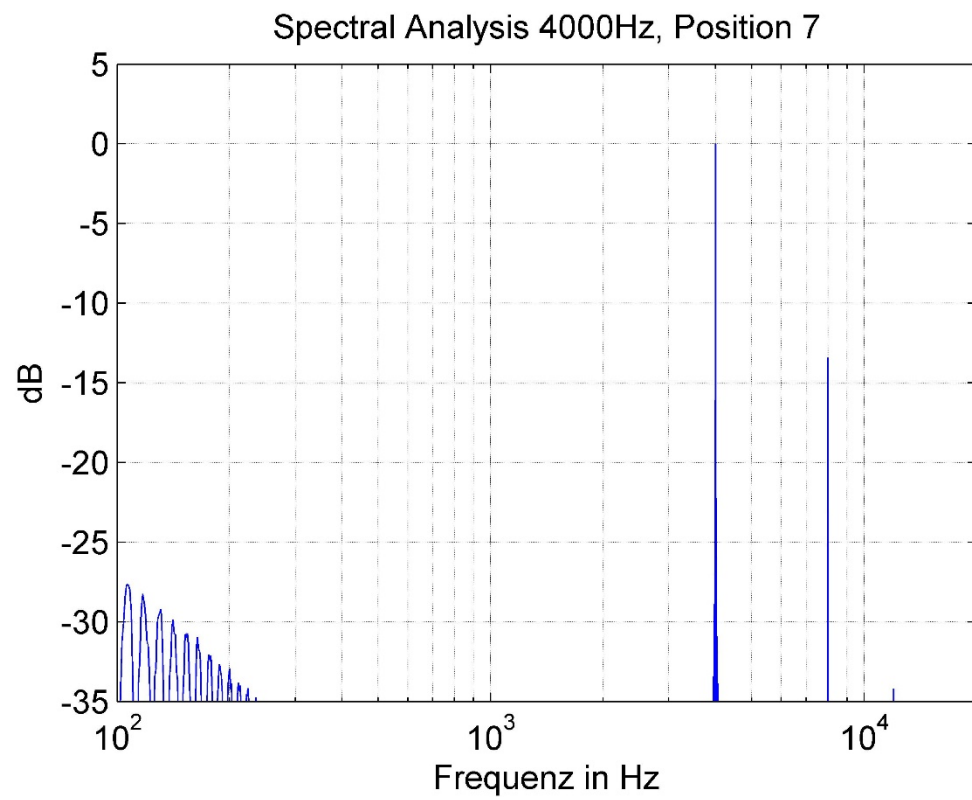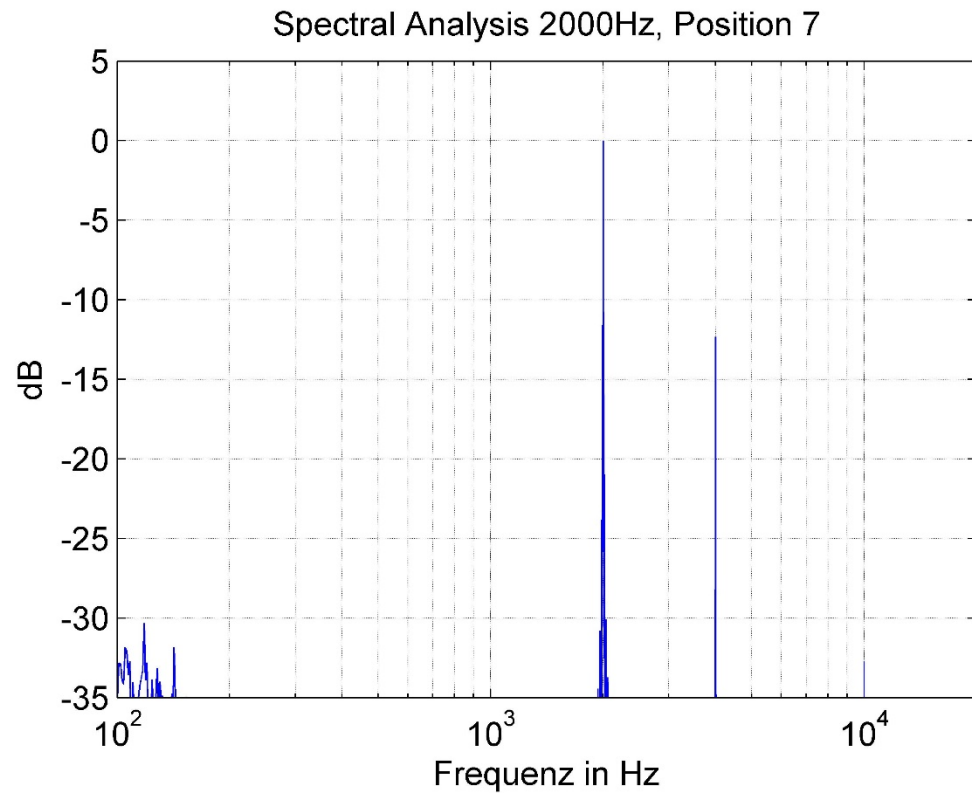
5.3.1. 2nd -Harmonic Distortion of Reproduced Acoustic Signal

According to the theory of chapter 2.2, a correct reconstruction of acoustic signal need always extra power, especially when the DC-offset method is applied. The measured efficiency should be the "true" efficiency including DC part. Therefore, spectral analysis for the 2nd-Harmonic should be conducted to check the quality of the reconstructed acoustic signal and if it agrees with the prediction of the theory.

Spectral Analysis 250Hz, Position 7

Spectral Analysis 500Hz, Position 7

Spectral Analysis 1000Hz, Position 7

Spectral Analysis 2000Hz, Position 7

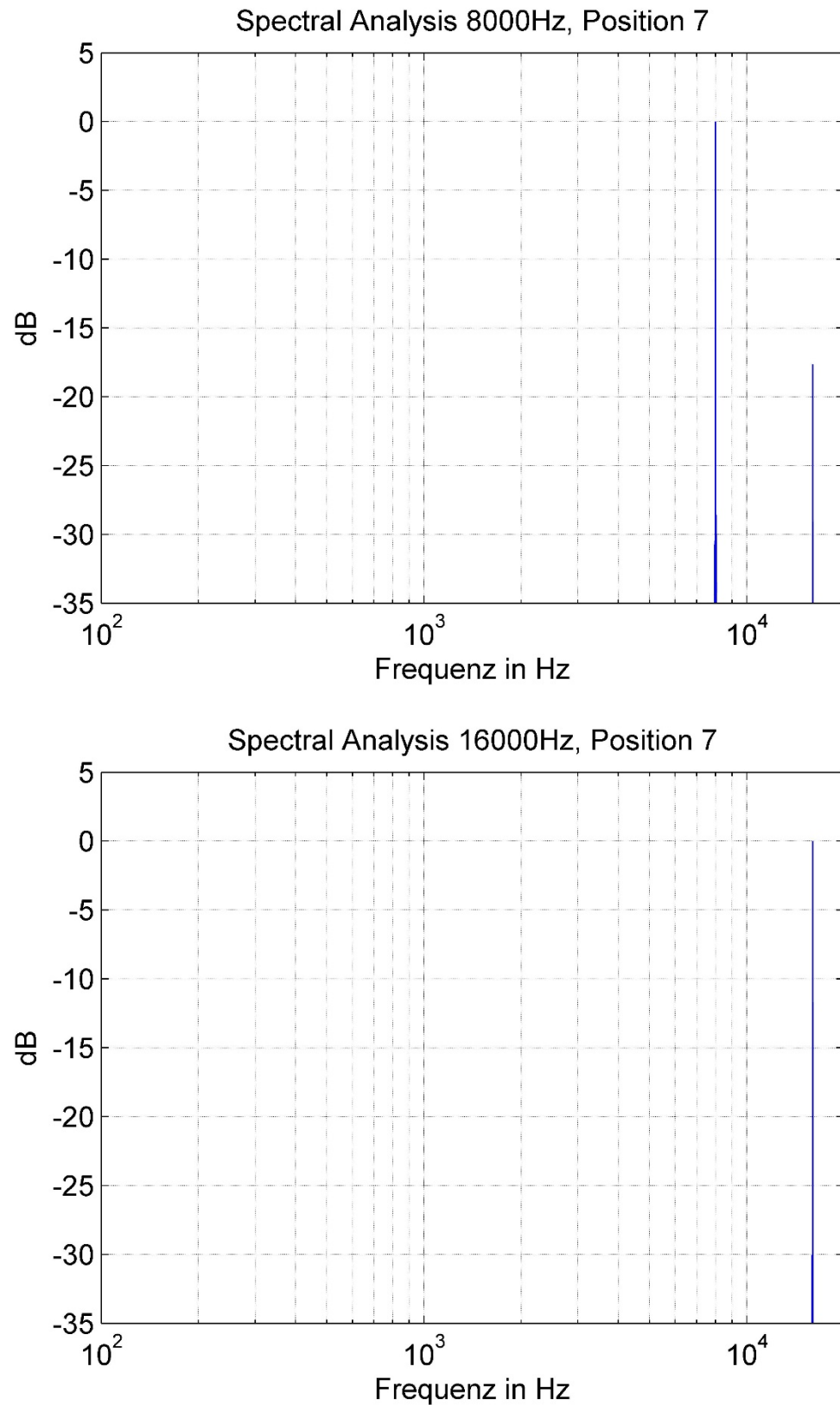## Spectral Analysis 4000Hz, Position 7

Figure 5.9 Spectral Analysis for DUT2, Position 7.

As shown as an example in Figure 5.9, the fundamental frequency has already been correctly reconstructed, along with residual 2nd -Harmonic frequency. Only for the fundamental frequency of 16 kHz, the 2nd -Harmonic is not depicted because 32 kHz is

already out of the Nyquist-frequency at the Sample rate of 48 kHz and out of the frequency response range of the Microphone as well.

For an Input of $U_{\text{ac,peak}} = 3.2\,V$ and $U_{\text{dc}} = 4\,V$, the theoretic ratio of fundamental signal to 2nd-Harmonic frequency should be:

$$20\lg\left(\frac{4U_{\text{dc}}}{U_{\text{ac,peak}}}\right) = 13.979\ \text{dB} \approx 14\ \text{dB}$$

Table 2 to Table 5 show the ratio of DUT1 to DUT4 in octave bands for every measuring point in dB and its discrepancy from the theoretical value in percentage.

Frequency (Hz)		250 dB	250 Δ	500 dB	500 Δ	1k dB	1k Δ	2k dB	2k Δ	4k dB	4k Δ	8k dB	8k Δ
p	1	15.21	8.78%	13.99	0.06%	12.09	-13.51%	12.56	-10.14%	10.74	-23.14%	18.54	32.66%
o	2	15.66	12.06%	14.14	1.13%	12.49	-10.62%	11.99	-14.25%	12.94	-7.44%	14.97	7.12%
s	3	15.70	12.32%	14.25	1.94%	12.30	-12.01%	12.56	-10.17%	12.81	-8.36%	14.70	5.13%
i	4	15.35	9.81%	14.54	3.99%	12.31	-11.97%	12.78	-8.61%	12.65	-9.52%	15.99	14.35%
t	5	14.25	1.93%	14.06	0.56%	12.87	-7.95%	11.61	-16.95%	11.04	-21.00%	17.31	23.82%
o	6	0.00	-100.00%	0.00	-100.00%	0.00	-100.00%	0.00	-100.00%	0.00	-100.00%	0.00	-100.00%
n	7	0.00	-100.00%	0.00	-100.00%	0.00	-100.00%	0.00	-100.00%	0.00	-100.00%	0.00	-100.00%

Table 2 Ratio of *f* to 2*f* of DUT1

Frequency (Hz)		250 dB	250 Δ	500 dB	500 Δ	1k dB	1k Δ	2k dB	2k Δ	4k dB	4k Δ	8k dB	8k Δ
p	1	13.97	-0.09%	15.38	10.03%	14.96	6.98%	12.43	-11.09%	13.38	-4.26%	16.80	20.18%
o	2	15.71	12.41%	15.13	8.24%	14.93	6.78%	11.51	-17.68%	14.81	5.96%	18.49	32.29%
s	3	15.35	9.83%	15.39	10.08%	14.41	3.08%	12.82	-8.31%	14.86	6.30%	21.10	50.91%
i	4	16.32	16.73%	14.84	6.18%	13.98	0.01%	13.41	-4.10%	14.03	0.39%	16.76	19.86%
t	5	15.89	13.69%	14.79	5.82%	13.97	-0.03%	12.78	-8.61%	13.59	-2.77%	17.18	22.92%
o	6	15.97	14.21%	14.60	4.43%	14.10	0.88%	13.20	-5.54%	13.68	-2.16%	17.14	22.61%
n	7	15.70	12.31%	14.97	7.10%	13.95	-0.23%	12.34	-11.75%	13.42	-4.02%	17.64	26.20%

Table 3 Ratio of *f* to 2*f* of DUT2

Frequency (Hz)		250 dB	250 Δ	500 dB	500 Δ	1k dB	1k Δ	2k dB	2k Δ	4k dB	4k Δ	8k dB	8k Δ
p	1	17.20	23.03%	14.20	1.57%	13.76	-1.60%	16.04	14.72%	10.79	-22.84%	19.78	41.49%
o	2	16.23	16.08%	15.01	7.35%	11.59	-17.06%	15.33	9.63%	18.63	33.29%	28.09	100.97%
s	3	17.42	24.62%	16.89	20.82%	9.36	-33.04%	18.82	34.61%	14.98	7.16%	25.16	80.01%
i	4	17.73	26.86%	16.34	16.89%	10.55	-24.53%	17.34	24.02%	13.31	-4.76%	22.09	58.04%
t	5	18.27	30.72%	17.20	23.04%	9.93	-28.94%	18.23	30.39%	12.28	-12.16%	21.26	52.08%
o	6	25.89	85.21%	18.19	30.16%	10.24	-26.78%	18.33	31.15%	17.84	27.63%	24.82	77.59%
n	7	18.27	30.69%	16.42	17.44%	10.35	-25.96%	18.36	31.35%	14.85	6.25%	22.43	60.44%

Table 4 Ratio of *f* to 2*f* of DUT3

Frequency (Hz)		250 dB	250 Δ	500 dB	500 Δ	1k dB	1k Δ	2k dB	2k Δ	4k dB	4k Δ	8k dB	8k Δ
p	1	18.64	33.31%	16.81	20.27%	12.99	-7.06%	15.25	9.08%	17.58	25.74%	23.14	65.50%
o	2	20.21	44.60%	17.80	27.34%	14.12	1.04%	13.40	-4.12%	15.27	9.27%	23.83	70.44%
s	3	20.77	48.55%	19.69	40.86%	14.63	4.63%	14.30	2.27%	21.20	51.66%	32.37	131.6%
i	4	19.65	40.57%	17.00	21.63%	14.63	4.67%	13.81	-1.19%	15.76	12.74%	22.86	63.53%
t	5	19.85	42.03%	17.95	28.40%	14.47	3.52%	13.48	-3.55%	14.55	4.06%	20.74	48.38%
o	6	19.70	40.93%	17.99	28.66%	14.60	4.45%	13.72	-1.82%	16.56	18.43%	27.03	93.39%
n	7	19.91	42.44%	17.75	26.99%	14.60	4.43%	13.36	-4.40%	14.70	5.16%	20.56	47.05%

Table 5 Ratio of *f* to 2*f* of DUT4

Though the theory does not consider the ratio being related to frequency, the ratio does differ from frequency to frequency and apparently depends on the folio physical properties. Since DUT1 and DUT2 are made from the same folio with lower density, the performance of these two is in generally better as DUT3 and DUT4, whose density is about four times higher. Nonetheless, this ratio affects mainly the quality of the reproduced acoustic signal, as for the measuring of efficiency, the ratio of all frequency and DUTs should be adequate.

5.3.2.   SPL in Octave Band
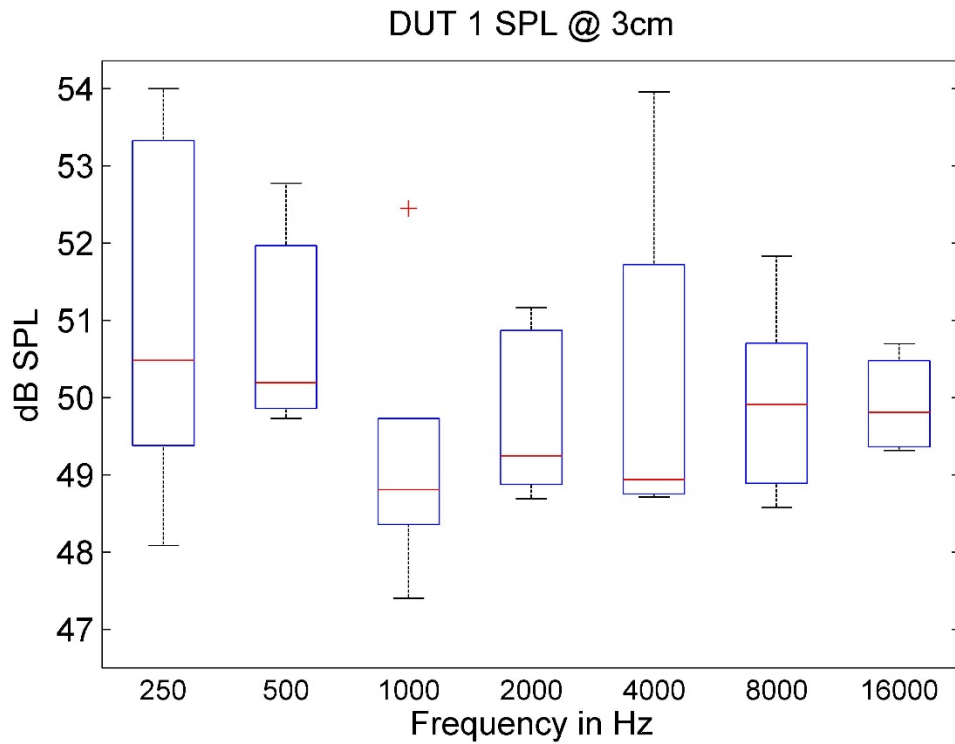
Figure 5.10 Time-averaged SPL of DUT1
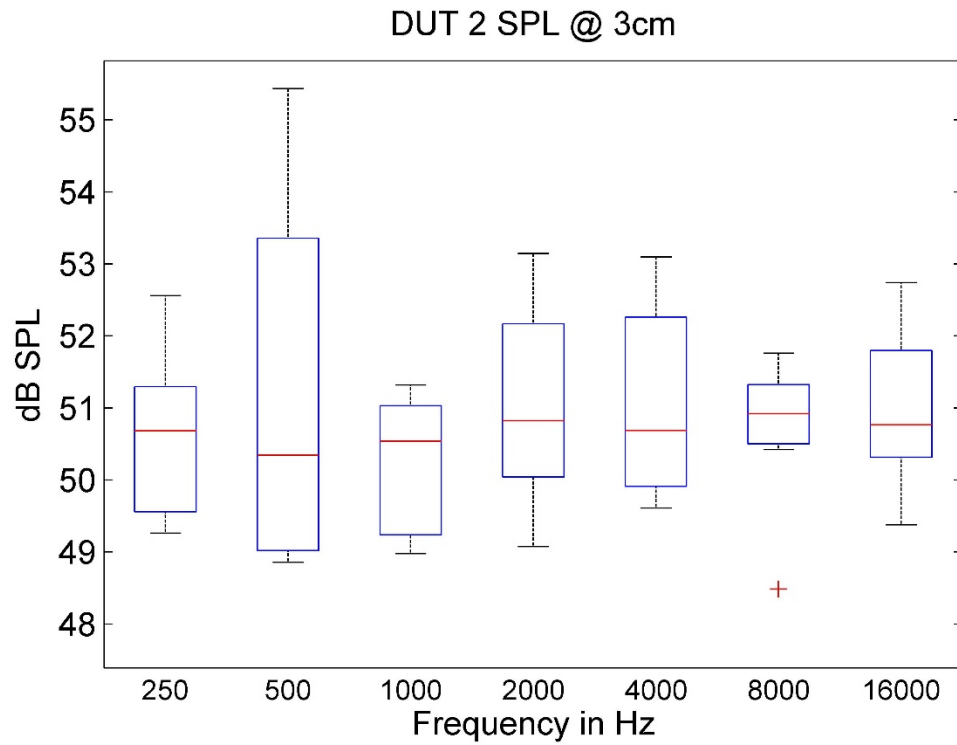
Figure 5.11 Time-averaged SPL of DUT2
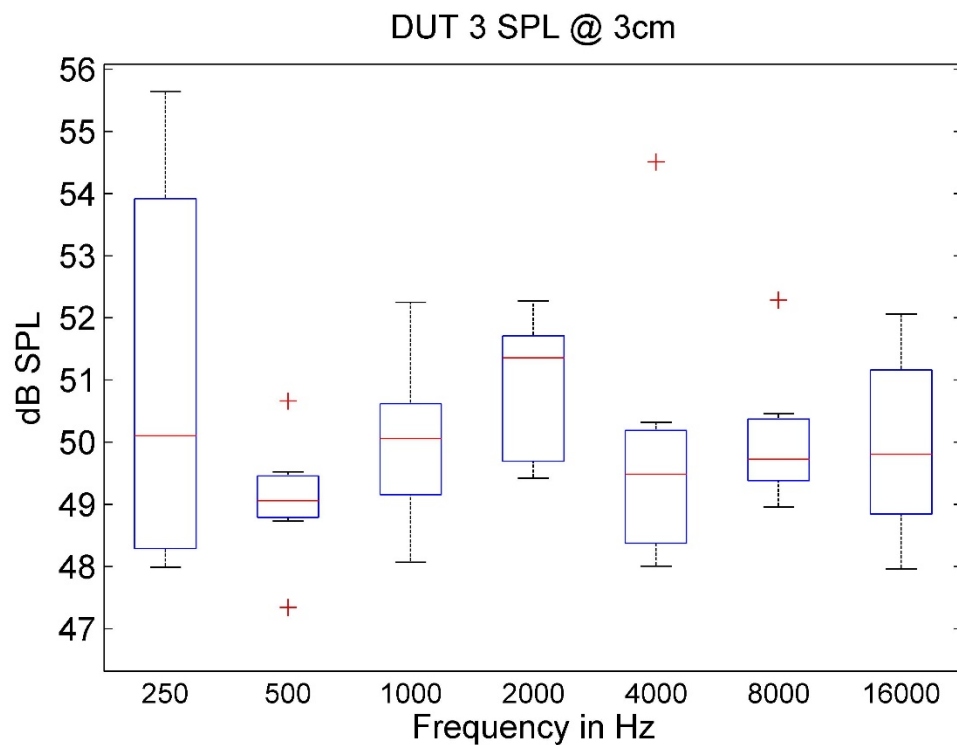
Figure 5.12 Time-averaged SPL of DUT3
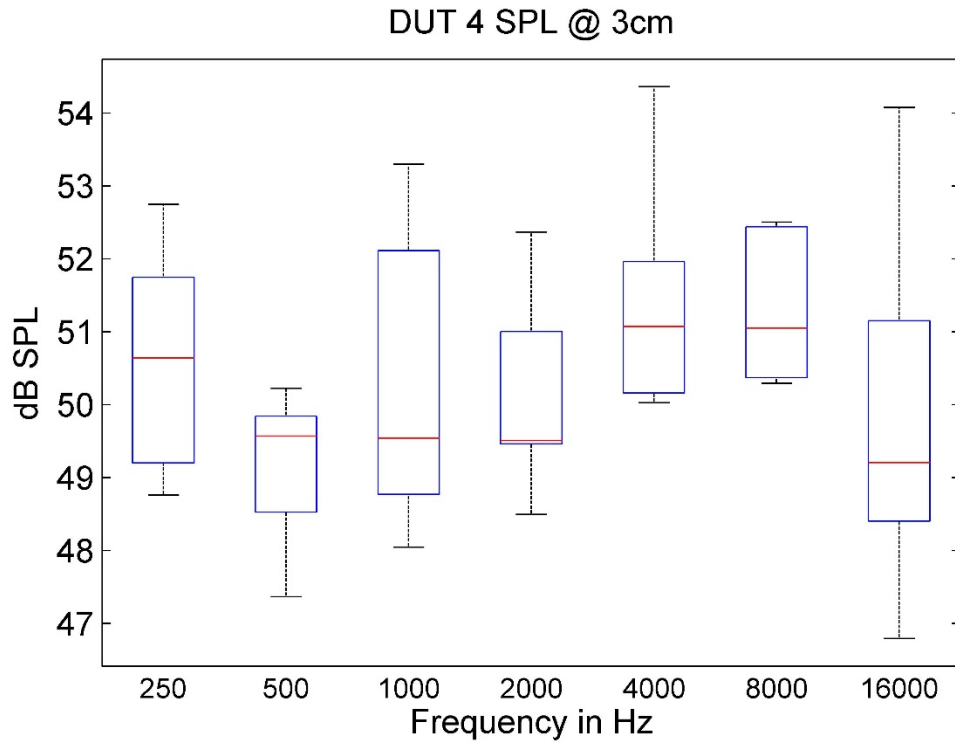
Figure 5.13 Time-averaged SPL of DUT4

Figure 5.10 to Figure 5.13 show the time-averaged SPL from all measuring angles, all taken at distance of 3 cm.

The time-averaged SPL is calculated using following equation:

$$L_{\text{eq}} = 10 \lg \left(\frac{1}{T} \int_0^T 10^{L(t)/10} \, dt \right) \tag{27}$$

For same frequency, the SPL shows a slight discrepancy in different angles, but between different frequencies, the extent of the discrepancy is also different, suggesting there is no extremely directional dependency for SPL. From the trends of median value for each DUTs, DUT2 seems to have the best performance; the sound pressure eradiates evenly for every frequency. On the other hands, DUT3 have the most abnormal values, suggesting there could be some structural defects which cause unstable performance for some frequencies.

5.3.3. Efficiency
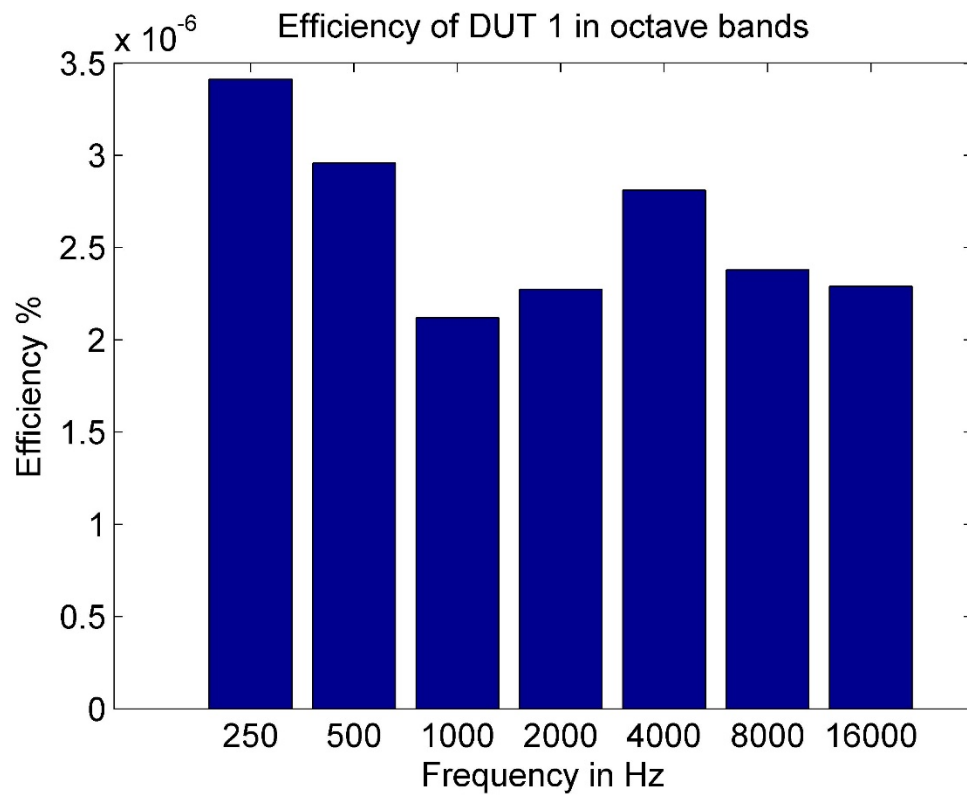
Figure 5.14 Efficiency of DUT1
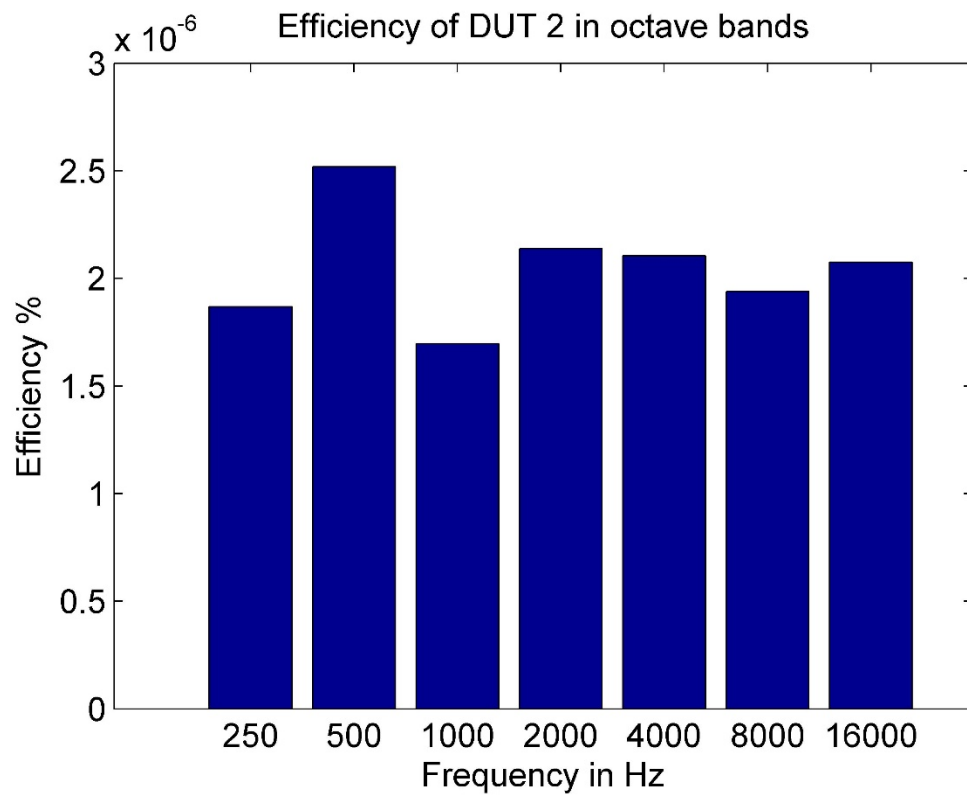
Figure 5.15 Efficiency of DUT2
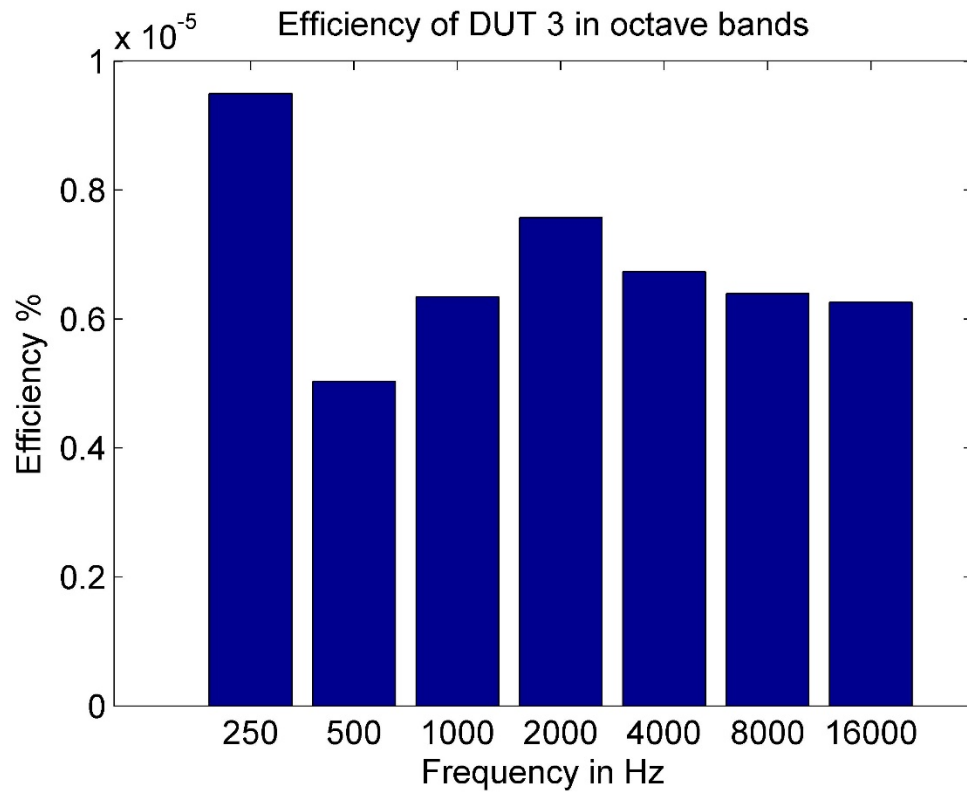
Figure 5.16 Efficiency of DUT3
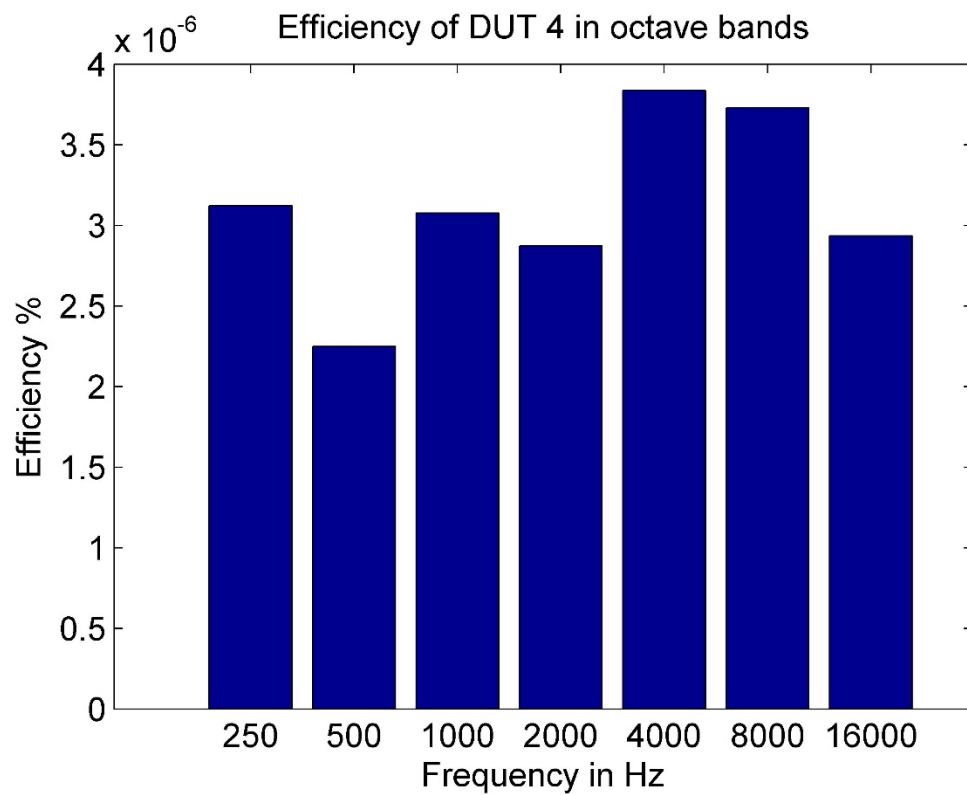
Figure 5.17 Efficiency of DUT4

Based on the correct reproduction of fundamental frequency the actual efficiency of every DUT is shown in Figure 5.14 to Figure 5.17.

In general, the efficiency of all frequencies falls in the range **between 1.5*10^(-6) % and 4.0*10^(-6) %,** except for DUT3. The efficiency of DUT3 is 2.25-2.6 times higher than other DUTs, due to exceptional high DC-resistance (around 400 ohm), which causes an exceptionally low electric power of DC by calculation. This could also be a side-effect of some structural defects.

The measured efficiency of DUT 1, DUT2 and DUT4 are however of the same magnitude as reported by (Tian et al., 2011) and (Suk et al., 2012). A summarize of efficiency for some thermoacoustic assemblies are also given by (Aliev et al., 2015)

5.3.4.   Comparing the Measured SPL with Theory
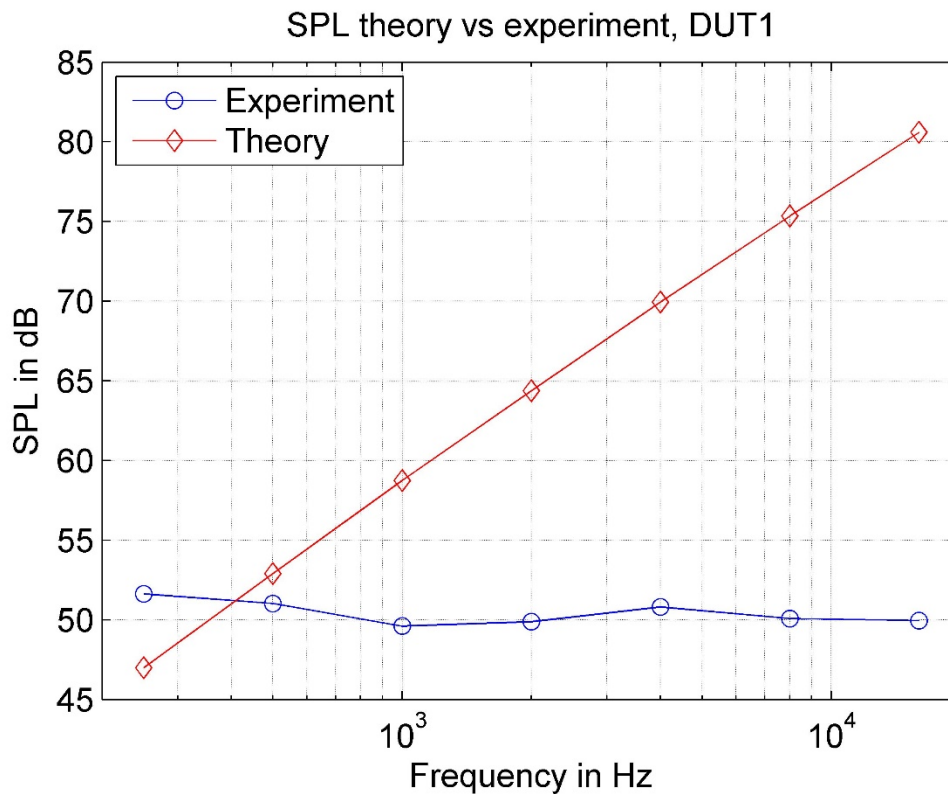
Figure 5.18 Theoretic SPL vs. Measured SPL for DUT1
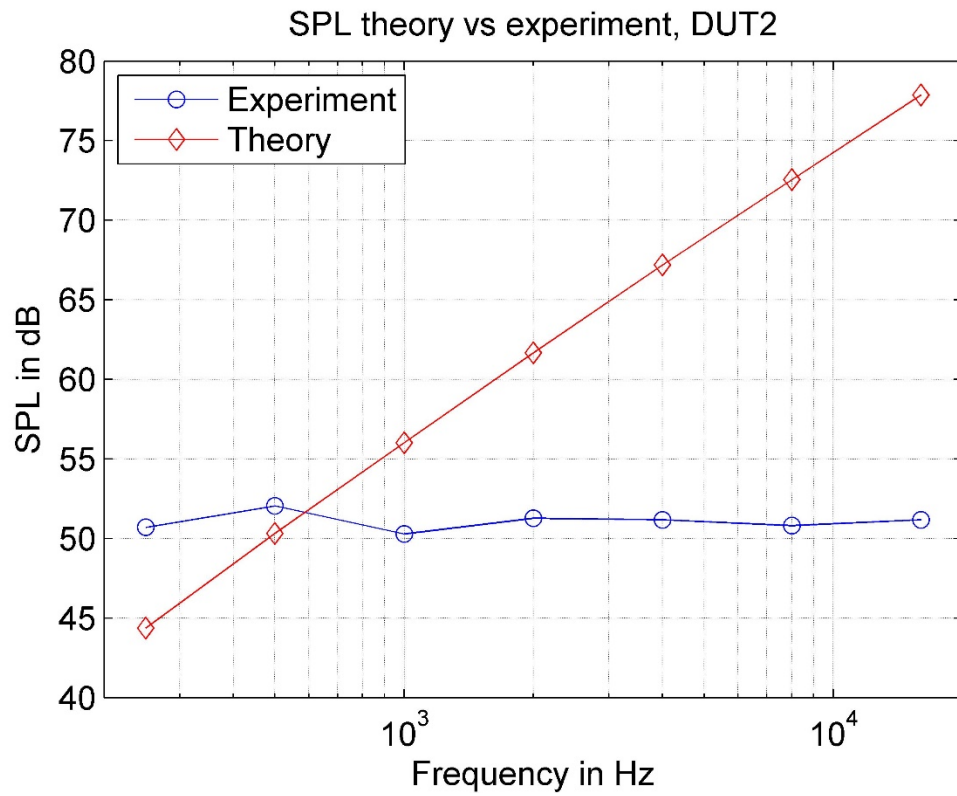
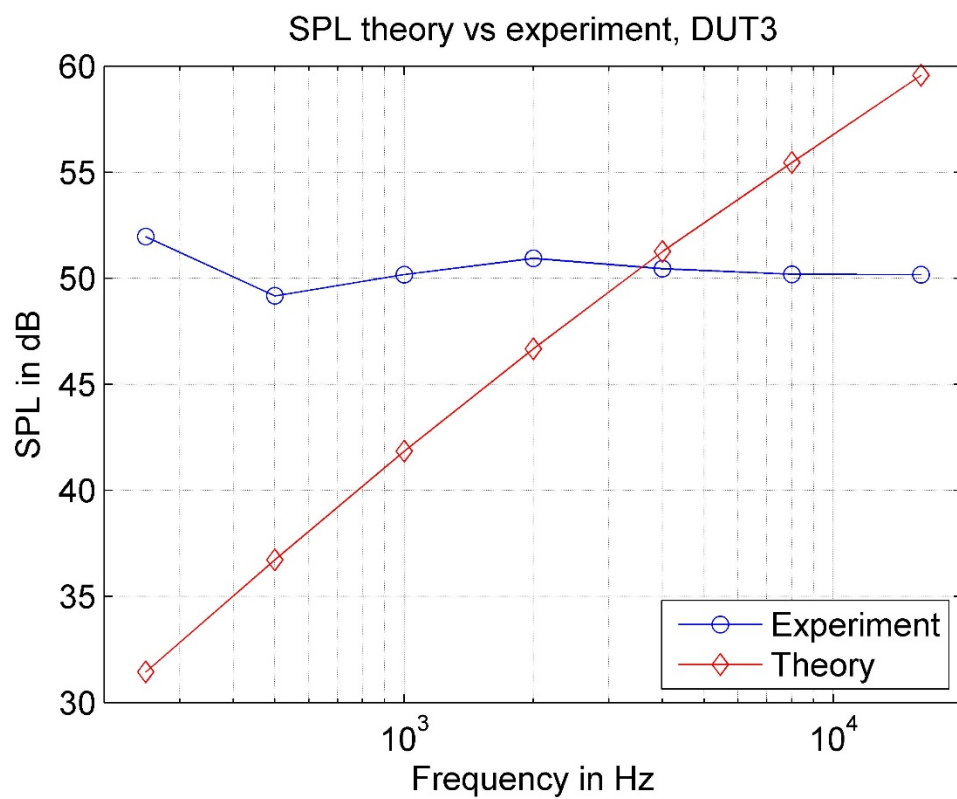Figure 5.19 Theoretic SPL vs. Measured SPL for DUT2

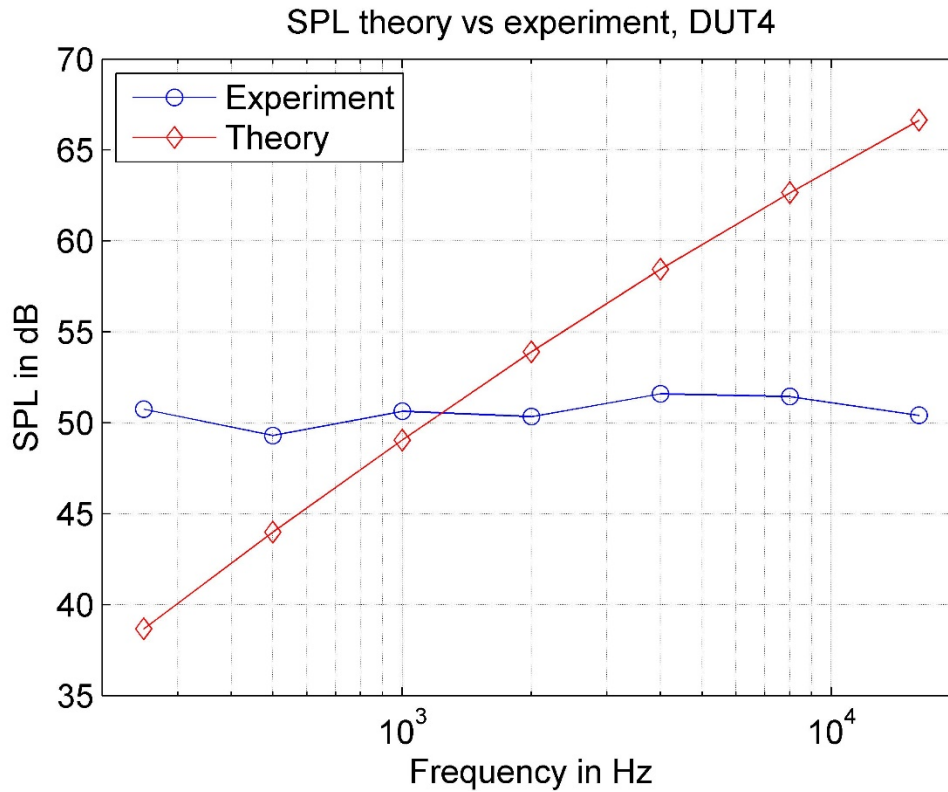Figure 5.20 Theoretic SPL vs. Measured SPL for DUT3

Figure 5.21 Theoretic SPL vs. Measured SPL for DUT4

The theoretic SPL is calculated according to Eq. (1), using the constants listed in Appendix 1 Table of Constants.
The critical frequencies for all DUTs are calculated as per Eq. (13):

DUT1 & DUT2: $f \gg 1.083$ MHz
DUT3 & DUT4: $f \gg 57.72$ kHz

Therefore, for theoretical calculation in the range of 250 Hz to 16 kHz, the additional coefficients cannot be omitted.

The proportional relation of sound pressure and the square root of frequency has however not been confirmed by the results of the experiment.

5.4. Error Analysis

5.4.1.   Reflection from Table Surface
    During the test, all DUTs are first installed into a foam base which is fixed on a table. The reflection of the table or other structures around could be a potential source of error since the calculation assumes of an entirely no reflection situation and an evenly spread sound intensity on an imaginal sphere (the direct field assumption). The extent of influence from reflection is however neglectable. First, the foam base is not a reverberant surface, the

reflection within the radius of the foam base should be minimized. Second, the distance between DUTs and the front end of the microphone is 3 cm which already smaller than the length of the foam. Even there is some reflection happens on the surface of the table, it would barely be picked up by the microphone since the path of reflections could not be once more altered in an anechoic chamber. Therefore, even considering the tiny reflection from the foam base, the results should not deviate much from that of the assumption.

5.4.2. Inaccurate Reading of Oscilloscope

The voltage level was observed and adjusted using an analog oscilloscope, some inaccurate reading of voltage from the waveform of the screen could exist since there are no other aiding tools, for instance, a cursor in a digital oscilloscope. The slight modulation of high frequency from the handmade circuit also deteriorate the clarity of waveform which also makes a more accurate reading of voltage peak still difficult.
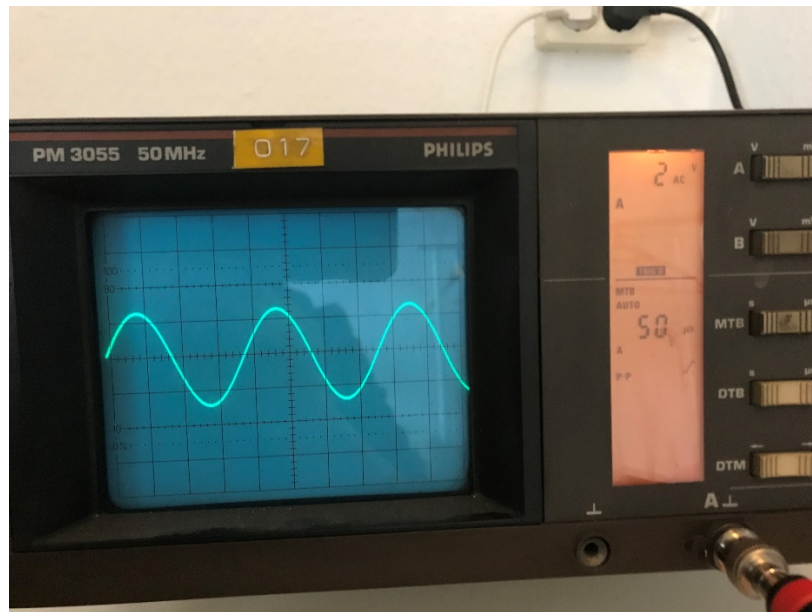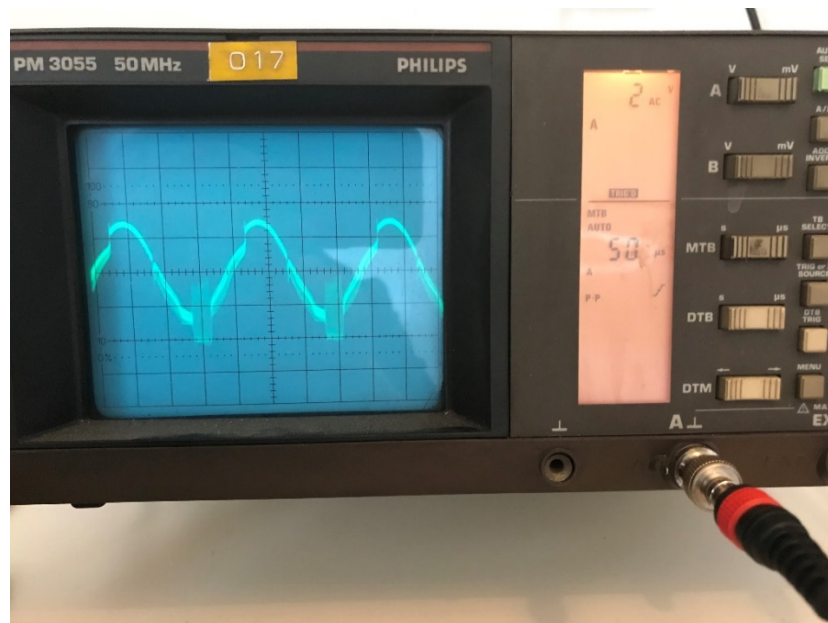
Figure 5.22 The Wave Form without Load

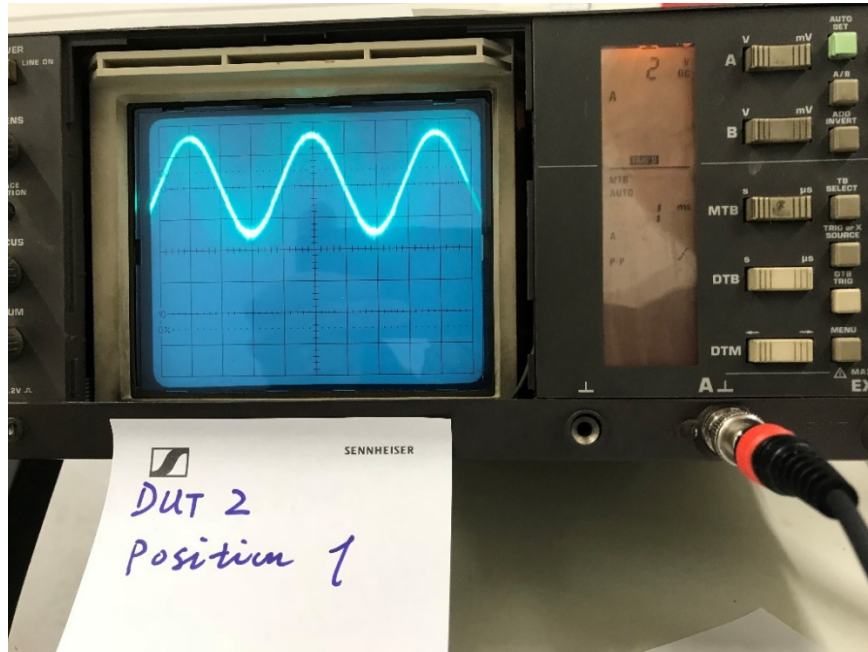Figure 5.23 Deteriorated Wave Form with Load

Figure 5.24 Improved Wave Form with Load (Using Bandpass Filter)

5.4.3.   Measure in Near Field

The far field condition has been mentioned in several articles (Asadzadeh et al., 2015) (Lim et al., 2013) (Fei et al., 2015) (Tian et al., 2011) (Tian et al., 2012), yet using another definition rather than those from classic acoustic theory.

Base on the theory from "Technische Akustik" (Möser, 2012), the measurement should be taken in the far field, which can be tested using following three conditions:

$$R \gg l$$
$$\frac{R}{l} \gg \frac{l}{\lambda}$$
$$R \gg \lambda$$

where

R: distance between microphone and center of the folio

l: height of the folio

λ: wave length

The following table calculates the upper and lower frequency limit using the geometric parameter of the folio during the test.

R	l	the lower limit of f	the upper limit of f
cm	cm	kHz	kHz
3	1	11.33	102
3	1.5	11.33	45.33
3	2	11.33	25.5

Table 6 Frequency Limit of Far Field According to Classic Acoustic Theory

Obviously, most of the tested frequencies are out of this range, according to this definition.

On the other hands, if the Rayleigh distance is introduced to distinguish the near field from the far field as done by many thermoacoustic experiments, the far field condition is very easy to be fulfilled.

Rayleigh distance is defined as follows:

$$R_0 = \frac{A}{\lambda}$$

where

A: area of folio

λ: wave length

The critical distance distinguishing near field from the far field are thus showed in Table 7.

f Hz	250	500	1000	2000	4000	8000	16000
A cm^2				4			
R_0 cm	0.029	0.059	0.118	0.235	0.471	0.941	1.882
A cm^2				2.25			
R_0 cm	0.017	0.033	0.066	0.132	0.265	0.529	1.059
A cm^2				2			
R_0 cm	0.015	0.029	0.059	0.118	0.235	0.471	0.941

Table 7 Rayleigh Distance for DUTs

The distance between the microphone and the center of the folio is always 3 cm, which should be considered in far field for all the cases.

Since there is so far no research comparing those two methods and proving which is more plausible for the thermoacoustic scenario, the extent of related error could not be quantitatively measured.

For the r-GO folio, the radiating energy of the transducer is extremely low, the total gain of the signal chain has been set to a very high level, which also results in a high level of the noise floor. Though a higher measure distance could fulfill both far field condition at the same time, the useful signal could be merged into the noise floor and could thus not easily be retrieved.

5.4.4.   Change of Impedance during Measuring

The temperature of the DUTs rises during each excitation. After several heating-cooling circuses, the impedance of the DUTs will also rise, from generally several tens ohms to several hundred ohms, depending on the temperature fluctuate, the density and the ability of the heat dispersion of the folio.
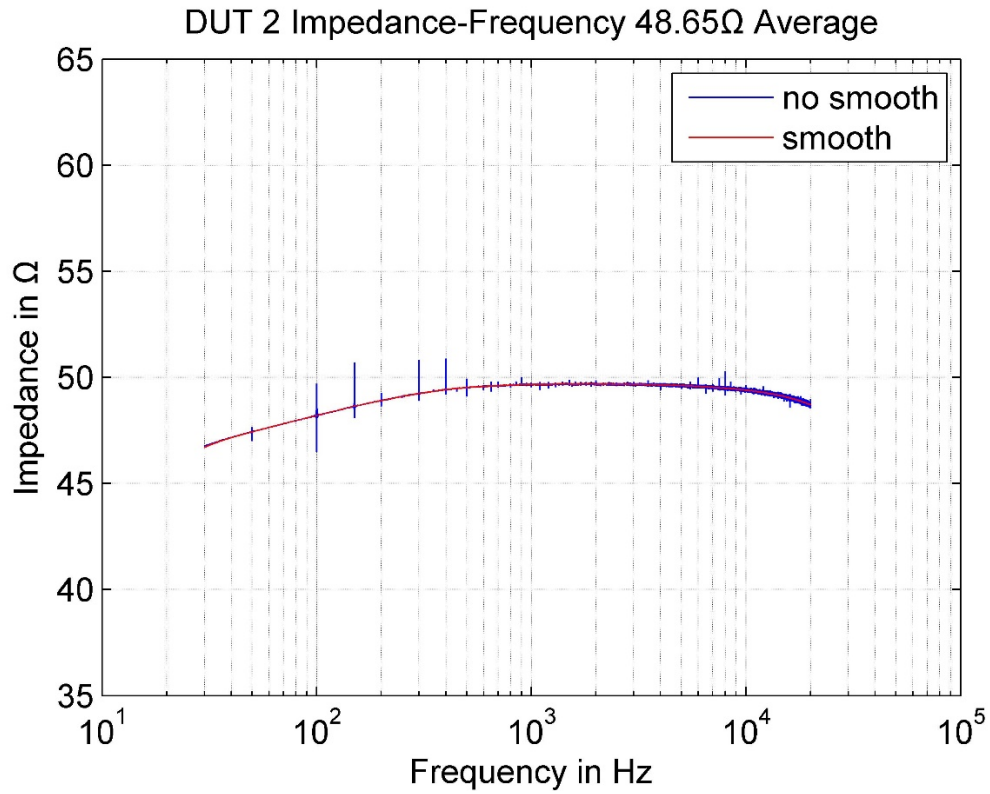
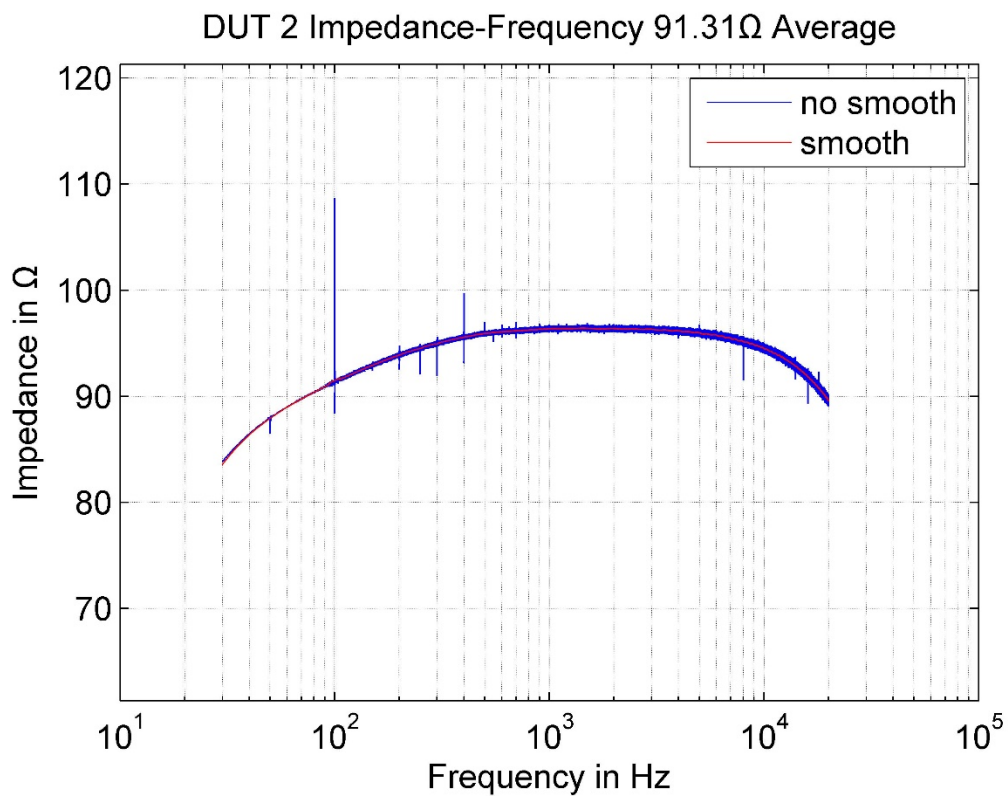Figure 5.25 Impedance Curve of DUT2 before Test

Figure 5.26 Impedance Curve of DUT2 after Test

Take DUT2 for example. It was loaded during the test under 3.2V peak AC voltage together with 4V DC voltage; the test lasted about 30 minutes. The average impedance level rises

from about 50 ohms to about 90 ohms. The shape of the curve keeps almost unchanged, indicating the total structure of the folio may still be intact.

The possible reason for such change could be:

- The expansion and contraction of the folio resulting from temperature fluctuation cause altering of the microstructure. The folio is a self-assembly structure from flakes of graphene stacking over each other. During the heating and cooling some of the flakes could be pushed away from each other by the changing of internal tension and therefore conducts no more current in those areas.

- The rising temperature causes incompletely oxidize on some area of the folio surface. Some graphene flakes could become CO or some other kinds of nonconductive oxide.

- The slight change of pressure between folio and electrodes due to expansion and contraction of the frame material.

In general, the conductive ability decreases with less conducting paths. The impedance increases thus apparently.
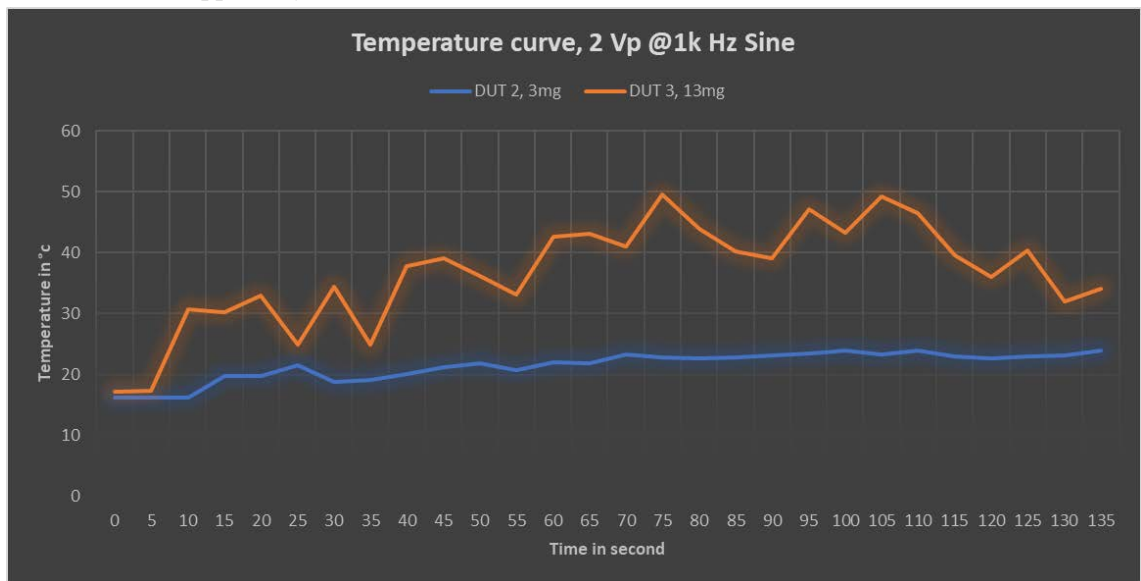
Figure 5.27 Temperature Curve of 2 min. Excitation

An additional temperature test shows in Figure 5.27. Even under 2 V peak voltage, the temperatures change in 2 minutes of 2 DUTs could be easily observed. Especially for DUT3 whose density is higher than DUT2 and thus thicker, the rising of temperature is more dramatical.

The detail of such interaction of temperature and impedance is yet unknown. However, for a more stable impedance, it seems lower density of the folio should be preferred.

6. Conclusion and Discussion

An assembly of r-GO in the form of paper like folio has been tested. According to the test result, this assembly can be used as a thermoacoustic transducer. The electroacoustic efficiency of 7 frequencies in octave band was tested using the reflecting plane method based on DIN EN ISO 3744 and falls in the range of $1.5*10^{\wedge}(-6)$ % to $4*10^{\wedge}(-6)$ %.

For the correct reconstruction of desired frequency and to minimize the 2nd- harmonic distortion, the DC-offset method was utilized.

For the calculation of the electric power of the folio, the impedance of the folio has been investigated using "I-V" method and proved to be mostly resistive within the audio frequency. It also confirms the theory of thermoacoustic that the acoustic phenomenon from the folio observed early in other experiment was not a result of vibration of the folio itself. Considering the almost pure and low resistive impedance across the acoustic frequency band, some difficulties may occur if driven by a conventional amplifier.

The measured SPL of different frequencies for one DUT is not proportional to $\sqrt{f}$. As predicted in Eq. (1), giving the same input electric power as well as same constants for surrounding medium and transducer itself, the root-mean-square of sound pressure should be proportional to $\sqrt{f}$. This discrepancy implies some hidden factors for the thermoacoustic theories have not yet been revealed.

The electroacoustic efficiency of this assembly is of the same magnitude as other assemblies using graphene in some early research. However, the efficiency is still not high enough for a practical audio transducer. Based on some theoretical calculation(Vesterinen et al., 2010), a higher electroacoustic efficiency could be achieved by further raising the input electric power, yet it is difficult for this folio structure. From the previous test using this folio, once the input voltage reaches $8 - 10$ V peak, some area of the folio turned red because of the extreme accumulation of heat and eventually caused permanent structural damage. Even though some of the folios survived from being damaged entirely, the impedance increased dramatically.

One possible explanation for the abnormal heat accumulation could be the multilayer structure of the folio since the folio was made by r-GO flakes pressing together into irregular layers. During the excitation, only several layers near the outer surface can transfer heat into surrounding air and thus produce sound pressure, while the heat from inner layers could not easily be transferred out and therefore can only keep heating the folio itself.

Figure 6.1 Multilayer Structure of folio and Heat Concentration (Red Area)

Furthermore, the thickness of the folio is not uniform; more heat will be produced at the part with more layers, where the temperature reaches the oxidizing temperature of carbon, and the surface becomes red. A folio with fewer layers may be therefore preferred for better performance and prevent damage. However, the thickness of the folio may be too low to maintain proper mechanical strength, and the folio could easily be cracked by force during the test. Despite such trade-off, it is quite essential that the waste heat consumed by inner layer should be lowered down for a better electroacoustic efficiency.

Another consequence of such structure is the unstable impedance. On the one hand, the multilayer structure could be altered by the heat-cooling cycle during working, as the inner tension in some area of the folio could be changed or the residual gas between layers expands and push layers away from each other. Some contacting layers could thus be disconnected and causing the impedance to increase. Sometimes tiny electric sparks were observed on the surface of the folio, indicating the direct contact between layers or between flakes in these areas has already been compromised.
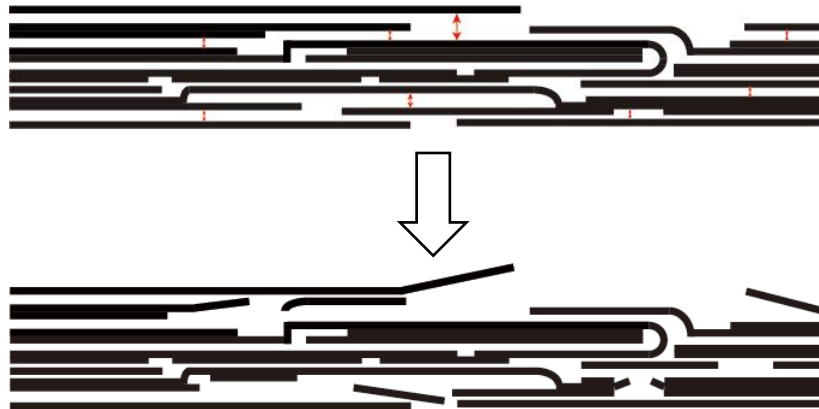
Figure 6.2 Structure altered by Tension or Gas Expansion

On the other hand, if the heat concentration in some area grows so high that some oxidation reaction could be triggered, some layers could be instantly destroyed, which also increases impedance. In some cases, extremely bright light along with smoke could be observed in those areas. In the worst case scenario, the folio could be damaged at the weakest point.

Figure 6.3 Structure Damaged by Oxidation (Red Line)

Other possible ways of improving the electroacoustic efficiency could be using some other signal processing methods instead of DC-offset, such as Amplitude Modulation of an Alternating Current signal(AMAC), Spectral Envelop Decimation of an Alternating Current signal(FCAC) and Linear Frequency Compression of an Alternating Current signal (TCAC) (Bouman, 2016); or improved DC-offset method using Square Root Circuit(Sugimoto and Nakajima, 2016). According to the theoretical calculation in Eq. (6) , there is always a considerable part of the input electric power being consumed by the direct current which has no contribution to the acoustic signal. Despite the easy implementation, the DC-offset method could be the most inefficient among others.

In this work, the measured SPL and efficiency of the thermoacoustic transducer using r-GO folio assembly are not yet comparable with the conventional acoustic transducer, i.e., electrodynamic transducer. The primary obstacle is the contradiction of a mechanically durable assembly and the energy wasted by acoustically unnecessary structures. Generally speaking, this kind of assembly is not suitable for high output power transducer, i.e., loudspeakers, but could be encapsulated into a small unit for low output scenario such as earphones. For such purpose the structure of assembly should be further evolved, keeping only the surface material for electro-thermo-acoustic conversion, and replacing inner layers with insulation and temperature insensitive material which does not consume electric power but only provides enough support for a durable structure. In this way, the assembly could also bear higher input power, which as the theory predicted could also increase efficiency performance. If the efficiency of improved assembly could ascend into the range of 10^{-5} % to 10^{-4} %, many practical applications could be expected to develop as a result.

Besides the application in the audible frequency range, the thermoacoustic transducer could be used for ultrasonic. The thermoacoustic transducer itself can easily double any given frequency and isn't affected by partial vibration like electrodynamic transducers because the thermoacoustic transducer is not a Mass-Spring system. Another advantage for an ultrasonic application is the proportional increase of efficiency to input frequency f, as per theoretical calculation in Eq.(1). Although this phenomenon has not been confirmed by this work, it is worth being re-tested in future research.

To summarize, the durability of the material should be further improved. One or more signal processing methods should be developed to cope with the 2nd-harmonic distortion efficiently for the audible application. The foundation of thermoacoustic should be more closely investigated for better explanation and guidance to future experiments.

7. Bibliography

Aliev, Ali E.; Nathanael K. Mayo; Monica Jung de Andrade; et al. (2015): „Alternative Nanostructures for Thermophones." In: *ACS Nano*, 9(5), S. 4743–4756.

Arnold, H. D. and I. B. Crandall. (1917): „The Thermophone as a Precision Source of Sound." In: *Physical Review*, 10(1), S. 22–38.

Asadzadeh, S. S.; A. Moosavi; C. Huynh; et al. (2015): „Thermo acoustic study of carbon nanotubes in near and far field: Theory, simulation, and experiment." In: *Journal of Applied Physics*, 117(9), S. 095101.

Bouman, Troy (2016): *DRIVE SIGNAL DEVELOPMENT FOR THE THERMOACOUSTIC LOUDSPEAKER*. Master Thesis, Michigan Technological University.

Brinkmann, Fabian und Stefan Weinzierl (2017): „AKtools—An Open Software Toolbox for Signal Acquisition, Processing, and Inspection in Acoustics." *Audio Engineering Society Convention 142*,.

Dikin, Dmitriy A.; Sasha Stankovich; Eric J. Zimney; et al. (2007): „Preparation and characterization of graphene oxide paper." In: *Nature*, 448(7152), S. 457–460.

DIN (2010): „Akustik — Bestimmung der Schallleistungs- und der Schallenergiepegel von Geräuschquellen aus Schalldruckmessungen — Hüllflächenverfahren der Genauigkeitsklasse 2 für ein im Wesentlichen freies Schallfeld über einer reflektierenden Ebene." *DIN EN ISO 3744: 2010*,.

Fei, Wenwen; Jianxin Zhou und Wanlin Guo (2015): „Low-voltage Driven Graphene Foam Thermoacoustic Speaker." In: *Small*, 11(19), S. 2252–2256.

Frank P. Incropera; Frank P. Incropera; David P. Dewitt; et al. (Hrsg.) (2007): *Fundamentals of heat and mass transfer*. 6th ed. Hoboken, NJ: John Wiley.

Li, Qin-Yi; Kailun Xia; Ji Zhang; et al. (2017): „Measurement of specific heat and thermal conductivity of supported and suspended graphene by a comprehensive Raman optothermal method." In: *Nanoscale*, 9(30), S. 10784–10793.

Lim, C.W.; L.H. Tong und Y.C. Li (2013): „Theory of suspended carbon nanotube thinfilm as a thermal-acoustic source." In: *Journal of Sound and Vibration*, 332(21), S. 5451–5461.

Marcano, Daniela C.; Dmitry V. Kosynkin; Jacob M. Berlin; et al. (2010): „Improved Synthesis of Graphene Oxide." In: *ACS Nano*, 4(8), S. 4806–4814.

Möser, Michael (2012): *Technische Akustik*. Berlin: Springer Vieweg.

Novoselov, K. S. (2004): „Electric Field Effect in Atomically Thin Carbon Films." In: *Science*, 306(5696), S. 666–669.

Sugimoto, Takehiro and Yoshiki Nakajima (2016): „Second harmonic distortion suppression of thermoacoustic transducer using square root circuit." In: *Acoustical Science and Technology*, 37(3), S. 99–105.

Suk, Ji Won; Karen Kirk; Yufeng Hao; et al. (2012): „Thermoacoustic Sound Generation from Monolayer Graphene for Transparent and Flexible Sound Sources." In: *Advanced Materials*, 24(47), S. 6342–6347.

Tian, He; Tian-Ling Ren; Dan Xie; et al. (2011): „Graphene-on-Paper Sound Source Devices." In: *ACS Nano*, 5(6), S. 4878–4885.

Tian, He; Dan Xie; Yi Yang; et al. (2012): „Single-layer graphene sound-emitting devices: experiments and modeling." In: *Nanoscale*, 4(7), S. 2272.

Vesterinen, V.; A. O. Niskanen; J. Hassel; et al. (2010): „Fundamental Efficiency of Nanothermophones: Modeling and Experiments." In: *Nano Letters*, 10(12), S. 5020–5024.

Xiao, Lin; Zhuo Chen; Chen Feng; et al. (2008): „Flexible, Stretchable, Transparent Carbon Nanotube Thin Film Loudspeakers." In: *Nano Letters*, 8(12), S. 4539–4545.

8. Figure List

9. Table List

10. Appendix 1 Table of Constants

The following table gives an overview of all constants used in this article:

Symbol	Name	Quantity	Unit	Condition
α	Thermal diffusivity of air	2.25×10^{-8}	m^2/s	Air at 300 K
β_0	The rate of heat loss per unit area of the folio (due to conduction, convection and radiation) per unit rise in temperature of the folio above that of its surroundings[8]	25	$W/m^2 \cdot K$	(Incropera et al., 2007)
$C_{P,\text{graphene}}$	The heat capacity per unit mass of graphene	700	$J/kg \cdot K$	(Li et al., 2017)
$C_{P,\text{air}}$	The heat capacity per unit mass of air	1.007×10^3	$J/kg \cdot K$	Air at 300 K
C_s	The heat capacity per unit area of folio	0.5859	$J/m^2 \cdot K$	DUT1 & 2
		2.5390		DUT3 & 4
ρ_0	Density of air	1.16×10^3	kg/m^3	Air at 300 K
κ	The thermal conductivity of air	2.63×10^{-2}	$W/m \cdot K$	Air at 300 K
T_0	The temperature of surrounding air	300	K	

---

[8] The calculated sound pressure is little sensitive to this constant, and for regular surface it mostly depends on the ambient gas. For the calculation in chapter 5.3.4 the upper limit for free convection of ambient gas is used as suggested in (Xiao et al., 2008).

11. Appendix 2 Digital Data

The following contents have been included in the attached CD-ROM (s):

1. this article in the form of pdf file.
2. Matlab® code for experiment and evaluation
3. Experiment data in M-format
4. Referenced Literatures